



The 2021 Atlantic Niño and Benguela Niño Events: external forcings and air–sea interactions

Serena Illig^{1,2} · Marie-Lou Bachelery³

Received: 9 June 2023 / Accepted: 18 August 2023
© The Author(s) 2023

Abstract

This paper presents a comprehensive analysis of the extreme Atlantic and Benguela Niño events that occurred during the boreal spring–summer of 2021. We conducted sensitivity experiments with a regional ocean–atmosphere coupled model of the tropical Atlantic to investigate the phenology of these interannual events, unravel their triggering mechanisms, and quantify the contributions of local and remote processes. The results revealed that both the 2021 Atlantic and Benguela Niños were triggered by anomalous atmospheric fluxes at the model southern boundary (32° S), leading to a significant and persistent weakening of the South Atlantic Anticyclone. The associated poleward anomalous coastal wind off Africa reduced coastal upwelling and evaporation south of 15° S, initiating the Benguela Niño. Then, the relaxation of the equatorial trade winds forced a downwelling equatorial Kelvin wave, which warmed the eastern equatorial region, marking the onset of the Atlantic Niño. The equatorial event reached full maturity in July 2021 through ENSO-like air–sea interactions in the equatorial basin, enhanced by the atmospheric connection associated with low-level winds converging toward the distant coastal warming. While air–sea interactions in the tropical Atlantic acted as a negative feedback for the coastal warming, the ocean connection with the equatorial variability through the propagation of equatorially-forced downwelling coastal waves intensified the coastal warming, peaking end of May 2021. Overall, this research provides valuable insights into the complex dynamics of Atlantic and Benguela Niños, emphasizing the interconnectedness between these two systems. This has important implications for improving Earth system models which currently struggle to simulate these extreme events.

Keywords Atlantic-Niño · Benguela-Niño · Air–sea-interactions · South-Atlantic-Anticyclone · Coastal-upwelling · Regional-coupled-modelling

Abbreviations

ABCs	Atmospheric Boundary Conditions	CROCO	Coastal and Regional Ocean COmmunity model
ATL3	[20° W–0° E; 3° S–3° N] domain	CTW	Coastal Trapped Waves
CARS2009	2009 CSIRO Atlas of Regional Seas climatology	DFS5.2	DRAKKAR Forcing Set v5.2
CABA	Coastal Angola Benguela Area ([2°-width coastal fringe, 10° S–20° S])	EKW	Equatorial Kelvin Wave
		MABL	Marine Atmospheric Boundary Layer
		SAA	South Atlantic Anticyclone
		SLA	Sea Level interannual Anomaly
		SLP	Sea-Level Pressure
		SST	Sea Surface Temperature
		SSTA	Sea Surface Temperature Anomaly
		SSS	Sea Surface Salinity
		STD	STandard Deviation
		WCEA	Western-Central Equatorial Atlantic ([40° W–20° W; 3° S–3° N])
		WRF	Weather Research and Forecast model

✉ Serena Illig
serena.illig@ird.fr

¹ Laboratoire d'Etudes en Géophysique et Océanographie Spatiale (LEGOS), CNRS/IRD/UPS/CNES, 14 av. E. Belin, 31400 Toulouse, France

² Department of Oceanography, MARE Institute, LMI ICEMASA, University of Cape Town, Rondebosch, Cape Town, South Africa

³ Geophysical Institute, University of Bergen and Bjerknæs Centre for Climate Research, Bergen, Norway

1 Introduction

The tropical Atlantic is a region influenced by strong ocean–atmosphere interactions that constrain its seasonal cycle and interannual variability. Among the most prominent features are the interannual Atlantic Niño (Carton and Huang 1994; Ruiz-Barradas et al. 2000; Servain et al. 2000; Lübbecke et al. 2018) and Benguela Niño events (Shannon et al. 1986; Florenchie et al. 2003; Imbol Koungue et al. 2019), which are characterized by anomalous warming of the Sea Surface Temperature (SST) in the eastern-equatorial (ATL3: [20° W–0° E; 3° S–3° N], Zebiak 1993) and southeastern Atlantic (CABA: [2°–width coastal fringe, 10° S–20° S], Illig et al. 2020) regions, respectively (see Fig. 1 for the boxes). In the eastern equatorial basin, Atlantic Niños are synchronized with the seasonal cycle, mostly apparent in the formation and the expansion of the cold tongue (Zebiak

1993; Burls et al. 2011; Keenlyside and Latif 2007). Meanwhile along the coasts of Angola and Namibia, Benguela Niños typically occur during the warm season, particularly in March/April/May before the onset of seasonal maxima (Florenchie et al. 2003, 2004). The spatial characteristics of these events during the boreal summer of 2021 are shown in Fig. 1a using satellite SST data. During the development and peak phases of the events, SST anomalies reached values of about 1.6 °C in both the equatorial and coastal sectors. These anomalous conditions can lead to a number of climatic and environmental impacts, including changes in rainfall patterns over the African continent (Hirst and Hastenrath 1983; Rouault et al. 2003, 2009; Mohino et al. 2011; Brandt et al. 2011; Lutz et al. 2015) as well as changes in the ocean productivity and fish stocks in the Angolan and Benguela upwelling systems (Gammelsrød et al. 1998; Binet et al. 2001; Boyer et al. 2001).

Although Atlantic Niños and Benguela Niños are similar in their characteristics, they are also inextricably linked by their forcing mechanisms. Both events are connected via an ocean connection associated with the equatorial dynamics (Hu and Huang 2007; Lübbecke et al. 2010; Illig et al. 2020). The modulation of the trade winds in the western part of the equatorial basin triggers Equatorial Kelvin Waves (EKWs), which propagate along the equatorial waveguide (Illig et al. 2004). During their propagation, the EKWs induce significant changes in the vertical and horizontal currents, resulting in significant temperature anomalies within the first 100 m of the eastern equatorial basin and potentially leading to the development of an Atlantic Niño event (Illig et al. 2006; Foltz and McPhaden 2010; Burmeister et al. 2016; Martín-Rey and Lazar 2019; Song and Aiki 2023). Once they reach the African continent, part of their energy is transmitted along the West African coast and propagates poleward as Coastal Trapped Waves (CTWs). Similar to EKWs, CTWs are associated with temperature anomalies along the west coast of Africa, which can give rise to a Benguela Niño event (Florenchie et al. 2004; Rouault et al. 2007, 2018; Imbol Koungue et al. 2017, 2019; Bachèlery et al. 2020). Notably, the westerly wind anomalies that trigger the initial EKWs at the origin of the Atlantic Niño development can be associated with cold conditions in the Pacific in the preceding spring, as was the case for the 1996 Atlantic Niño (Handoh and Bigg 2000; Illig et al. 2006). Cold conditions in the Pacific may foster a change in the Walker circulation over the Pacific–Atlantic, ultimately leading to anomalous wind events in the west-equatorial basin and consequently forcing downwelling EKWs, consistent with Colberg et al. (2004) and Münnich and Neelin (2005).

While it has been accepted that the ocean wave dynamics is detrimental to the generation of Benguela Niño events (Imbol Koungue et al. 2017, 2019; Bachèlery et al. 2016, 2020; Martín-Rey et al. 2018; Illig et al. 2020; Song et al.

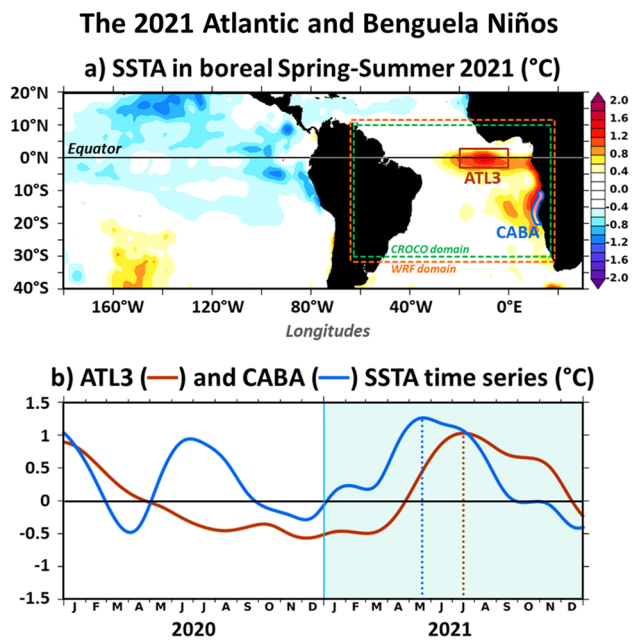


Fig. 1 Observed interannual SST anomalies (SSTA, °C) calculated over the period 2012–2021 from weekly OISST observations (Huang et al. 2021). **a** Map of the tropical Pacific–Atlantic with dashed rectangles delineating our regional tropical Atlantic Ocean (CROCO, green) and Atmosphere (WRF, orange) model domains. Within our model grids, the SSTA is averaged over the peak phase of the 2021 Atlantic and Benguela Niño events (June–July 2021), while outside the tropical Atlantic sector, previous SSTA conditions are averaged in May 2021. **b** Time series of the eastern equatorial (ATL3 box, [20° W–0° E; 3° S–3° N], red) and coastal (CABA box, average within a 2°-wide coastal band from 20° to 10° S, blue) SSTA for the years 2020 and 2021. The peaks of the 2021 Atlantic and Benguela Niños are highlighted with dotted vertical lines. The shaded cyan area represents the period during which we conducted our forced and coupled sensitivity experiments. The figure has been realized using the Ferret program (<http://ferret.pmel.noaa.gov/Ferret/>)

2023), several studies have also pointed to the direct influence of the local atmospheric forcing (Junker et al. 2015; Richter et al. 2010). Among them, Richter et al. (2010) suggest that SST anomalies in the CABA are not only preceded by westerly surface wind anomalies at the equator, but also by northerly wind stress anomalies off the African coast. Off the coasts, alongshore wind anomalies can trigger SST anomalies through local processes: locally forced CTWs, evaporation, and changes in the upwelling intensity. This atmospheric forcing plays a role in modulating the timing and the amplitude of the Benguela Niño events, either if it is in phase or out of phase with the oceanic wave dynamics (Bachèlery et al. 2016). Interestingly, Sea-Level Pressure (SLP) analyses show that a weakening of the South Atlantic Anticyclone (SAA) during the development phase of the Atlantic and Benguela Niños can trigger a weakening of the wind stress off the coast of Angola and in the west-equatorial Atlantic (Richter et al. 2010; Lübbecke et al. 2010, 2014). According to this paradigm, both the local atmospheric and the oceanic remote forcing are then related to the SAA forcing (Shannon and Nelson 1996; Hu and Huang 2007; Lübbecke et al. 2010).

The close relationship between Atlantic Niño and Benguela Niño events remains an active area of research. In particular, the question of how Atlantic Niños and Benguela Niños interact and whether they are part of a single mode of variability of the tropical Atlantic is still being debated among researchers. One intriguing aspect is their respective timing. While both events are dynamically connected by wind anomalies in the east-equatorial Atlantic that drive the propagation of EKW and subsequent CTW, Benguela Niños tend to occur about 1–3 months before Atlantic Niños (Hu and Huang 2007; Lübbecke et al. 2010; Polo et al. 2008; Illig et al. 2020). Motivated by the explanation of this inconsistent delay, two studies have brought to light another level of connection between the variability in the two regions. Hu and Huang (2007) suggested that the east-equatorial and southeastern warm events interact with each other through both, oceanic wave dynamics and large-scale atmospheric wind response: the warming initiated in the CABA triggers air–sea interactions that enhance the westerly wind anomalies in the equatorial Atlantic, which then causes the Atlantic Niño event. In return, the SST anomalies in the cold tongue weaken the SST anomalies off the Angolan coast by modifying the direction of the alongshore winds. The evolution and the complex interplay between the two events has been further highlighted by a recent study by Illig et al. (2020). Using idealized forced ocean model experiments, the authors demonstrate that the timing of the coastal event is directly related to the amplitude of the Atlantic Niño. The warming in the east-equatorial sector induces the development of a convergent circulation over the cold tongue, which

amplifies the upwelling-favorable coastal winds off the African coast and provoke the early demise of the warm SST anomalies there. The results of Illig et al. (2020) imply that the SST variability in the cold tongue, in phase with its seasonal cycle, may influence the local forcing along the coast of southwestern Africa through ocean–atmosphere coupling in the equatorial band, which in turn controls the magnitude and timing of the coastal events. However, this link could not be tested because it requires the use of ocean–atmosphere coupled model simulations in which ocean conditions can affect surface momentum and heat fluxes.

In this context, the 2021 Atlantic and Benguela Niño events are of particular interest. These events followed exactly the sequence described in Illig et al. (2020), with the Benguela warm event peaking in May, 2 months before the anomaly reaches its full values in the eastern-equatorial sector (Fig. 1b). It is interesting to note that the events of 2021 developed during moderate La Niña conditions, as shown in Fig. 1a, a warmer than usual North tropical Atlantic (WMO No. 1300 2022). This may have created the right conditions for the development of the wind anomalies in the west-equatorial Atlantic and thus triggered the Atlantic Niño events, as suggested in Illig et al. (2006). The aim of this study is to go beyond the limitations of Illig et al. (2020) by developing regional coupled ocean–atmosphere simulations of the South tropical Atlantic. We will base our study on the 2021 case, as it provides the right benchmark to investigate the oceanic and atmospheric linkages between the two events. Our objectives are to describe the phenology of these interannual events, unravel their triggering mechanisms, and quantify the contributions of local and remote processes. The results will contribute to a better understanding of the ocean–atmosphere interactions between tropical and south-east Atlantic variability, and in particular to assess whether Benguela Niños can influence the westerly wind anomalies in the equatorial Atlantic and support the development of Atlantic Niños as suggested by Hu and Huang (2007).

The paper is organized as follows: In Sect. 2, we introduce the tropical Atlantic regional ocean–atmosphere coupled model configurations and present the forced and coupled experiments conducted. A validation exercise of the model components in forced and coupled contexts is provided in the Supplementary Material. Section 3 analyzes the 2021 Atlantic and Benguela Niño events and the observed basin-scale anomalous conditions. Sensitivity experiments in a forced context allow to quantify the atmospheric response associated with the SSTA from that associated with the atmospheric fluxes entering and exiting the tropical Atlantic. In Sect. 4, we use coupled simulations to investigate the triggering mechanism and examine the air–sea interactions at work during the extreme events. Section 5 provides a discussion, followed by concluding remarks.

2 Tropical Atlantic Ocean atmosphere coupled model simulations, interannual anomalies, and key regions

2.1 The coupled model components

CROCO ocean component the Coastal and Regional Ocean Community model (CROCO; Shchepetkin and McWilliams 2005; Penven et al. 2006; Debreu et al. 2012) tropical Atlantic Ocean model configuration is similar to that developed in Illig et al. (2020), except that it is based on version 1.2 of CROCO. We use a third-order upstream biased scheme for momentum and tracer advection (Shchepetkin and McWilliams 1998). The subgrid vertical mixing is parameterized using a K-profile boundary layer parameterization scheme (Large et al. 1994) and defines the mixed layer depth. The domain extends from the east coast of South America to the west coast of Africa, from 30° S to 10° N at a resolution of 1/12° (Fig. 1), with 37 terrain-following vertical levels stretched near the surface. The bathymetry is derived from the GEBCO_08 30" elevation database (<http://www.gebco.net>) and the northern/southern open lateral boundary conditions are from the CARS2009 climatology (Dunn 2009; Ridgway et al. 2002). Because river discharges are not explicitly considered, the model Sea Surface Salinity (SSS) is restored to the CARS2009 monthly climatological SSS with increased restoration coefficients in the coastal areas. The model time step is 900 s.

For all the simulations performed, we store daily averages of the CROCO 2D-surface state variables (temperature, currents, and sea-level), while the 3D-variables and surface momentum/heat/freshwater flux are averaged every 3 days.

The WRF atmospheric component The atmospheric component is the Weather Research and Forecast (WRF) model version 4.1.3 (Skamarock et al. 2008, <http://www2.mmm.ucar.edu/wrf/users>), implemented in a 1/4° spatial configuration encompassing the ocean domain from 63.5 W to 18.5° E and from 32.08° S to 12.02° N to avoid the effect of WRF's sponge (Fig. 1). The vertical grid has 50 terrain-following levels, with a surface and upper stretch factors of 1.3 and 1.1, respectively. The model configuration was set-up with the following parameterizations: the WRF single-moment 6-class microphysics scheme (Hong and Lim 2006) modified to take into account the droplet concentration (Jousse et al. 2016); the new Goddard scheme for shortwave and longwave radiations (Chou and Suarez 1999); the Mellor–Yamada–Nakanishi–Niino (MYNN2.5) planetary boundary layer scheme (Nakanishi and Niino 2004); the Noah land–surface model; and the Mellor–Yamada–Nakanishi–Niino—Eddy–Diffusiv-

ity–Mass–Flux surface layer scheme (Nakanishi and Niino 2009; Olson et al. 2019). Cumulus are parameterized using the new simplified Arakawa–Schubert convection scheme from NCEP (Han and Pan 2011; Lim et al. 2014). 3-h ERA5 data (Hersbach et al. 2020) are used to initialize the model and to force it at the lateral open boundaries. The model time step is 90 s.

For all the simulations carried-out with WRF, the association with the XIOS library allows for saving hourly means of 2D fields (10 m-winds, precipitations, and heat/water surface fluxes) and daily means of 3D fields (winds).

The ocean–atmosphere coupling The Ocean Atmosphere Sea Ice Soil coupler version 4.0-MCT (OASIS-MCT, Craig et al. 2017) is used to exchange and regrid fields between CROCO and WRF on an hourly basis. In all our CROCO-WRF simulations, CROCO sends its SST to WRF, while WRF sends the surface wind-stress, the solar and net heat fluxes, and the evaporation-minus-precipitation field to CROCO. All exchanged fields are stored on both CROCO and WRF grids.

For the purpose of this study, we have added new features to the coupling strategy developed in CROCO. We have implemented the possibility to use coupling masks which allow to select the geographical regions in which the CROCO model is forced and/or coupled to WRF and allow to dissociate the dynamical (wind stress) or thermosaline (heat/freshwater fluxes) couplings. We can thus perform forced simulations in which a forced CROCO model sends its SST to WRF and in the meantime retrieve the atmospheric response from the coupler exchanged fields which are not used by CROCO (Sect. 2.2). We can also run fully coupled simulations in which we can keep the restoration of the observed SSS (Sect. 2.3). Ultimately, these developments will allow us to decouple regions where ocean waves are remotely forced (western equatorial Atlantic) from regions where ocean–atmosphere interactions appear to be critical for the timing of coastal events (eastern equatorial Atlantic and west African coastal band, see Illig et al. 2020).

2.2 CROCO-WRF Forced Simulations

First, a realistic interannual ocean simulation (CROCO^{INTER}, see Table 1) is run with the CROCO ocean model alone. Momentum, heat, and freshwater forcing fluxes are calculated using the COARE 3.0 bulk formulas (Fairall et al. 1996) using the atmospheric surface fields from the 3-h ERA5 reanalysis. To minimize biases in the mean state, the 10 m winds and the short- and long-wave radiations were previously corrected using the methodology developed to create the DRAKKAR Forcing Set v5.2 (DFS5.2, Dussin et al. 2016): To correct for the weak gyre circulation, the mean state of the surface winds was adjusted to relate to the 2000–2008 QuikSCAT mean wind amplitude (CERSAT

Table 1 Set of forced model experiments: Name of the experiment, design of the forced experiment (CROCO only or CROCO forcing WRF), period of the simulations, origin of CROCO restart, CROCO

surface forcing (include or not interannual frequencies), WRF Atmospheric Boundary Conditions (ABCs, include or not interannual frequencies), and number of ensemble simulations

NAME	Design	Period	Restart	CROCO surface forcing	WRF ABCs	Ens. Sim
CROCO ^{INTER}	CROCO only	2012–2021	CARS2009	Interannual	N/A	1
↔ Spawn CROCO ^{INTER-2020}		2020	CROCO ^{INTER}	Interannual	N/A	5
CROCO ^{CLIM}	CROCO only	2012–2021	CARS2009	Climatological	N/A	1
↔ Spawn CROCO ^{CLIM-2020}		2020	CROCO ^{CLIM}	Climatological	N/A	5
$\mathcal{F}^{\text{INTER}}$	CROCO $\xrightarrow{\text{SST}}$ WRF	2021	CROCO ^{INTER-2020}	Interannual	Interannual	5
$\mathcal{F}^{\text{CLIM-O}}$	CROCO $\xrightarrow{\text{SST}}$ WRF	2021	CROCO ^{CLIM-2020}	Climatological	Interannual	5
\mathcal{F}^{MEM}	CROCO $\xrightarrow{\text{SST}}$ WRF	2021	CROCO ^{INTER-2020}	Climatological	Interannual	5
$\mathcal{F}^{\text{CLIM}}$	CROCO $\xrightarrow{\text{SST}}$ WRF	2021	CROCO ^{CLIM-2020}	Climatological	No interannual	5

2002). To improve the mean cloud cover representation, the solar radiation is reduced and the incoming longwave radiation is increased using rectification coefficients estimated using DFS5.2 fields as our reference. Note that, since our configuration had already been implemented with a restoration to the observed SSS, we have not corrected the precipitation field. The model reaches a statistical equilibrium after 5 years of spin-up, which is performed by forcing the model from 2007 to 2011, starting from initial conditions derived from CARS2009 data. The CROCO^{INTER} simulation is then run over the 10-year period spanning from 2012 to 2021.

To smooth the intrinsic nonlinearities of CROCO in 2021, we spawn CROCO^{INTER} into 5 ensemble simulations (CROCO^{INTER-2020}, see Table 1). To do this, the model temperature is noised on January 1, 2020 using normally distributed random values with a 10^{-2} °C STD (as in Illig et al. 2020). These simulations spread-out throughout the year 2020 (see Fig. S2a, d in the Supplementary Material). The 5 ensemble simulations are continued throughout the year 2021, during which their hourly SSTs serve as WRF surface boundary conditions, thus forming 5 atmospheric ensemble simulations in which the Atmospheric Boundary Conditions (ABCs) include interannual forcing (see Sect. 2.1). These interannual forced ocean–atmosphere ensemble simulations are called $\mathcal{F}^{\text{INTER}}$ (Table 1) and their ensemble mean will allow for the analysis of both the ocean dynamics and its atmospheric response (Sect. 3.1).

To estimate the 2021 interannual ocean and atmospheric anomalies of $\mathcal{F}^{\text{INTER}}$, we have designed a climatological experiment ($\mathcal{F}^{\text{CLIM}}$, see Table 1) that provides the mean state from which the anomalies deviate. In $\mathcal{F}^{\text{CLIM}}$, CROCO is forced by the 2012–2021 monthly climatological surface forcings estimated from CROCO^{INTER}, and at WRF lateral open boundaries, the interannual variability has also been filtered out. It is worth mentioning that the diurnal cycle is preserved in both the ocean and the atmospheric forcing. To ensure sufficient energy input into the coupled system, the intraseasonal fluctuations of the fluxes entering and exiting

the WRF domain are conserved in WRF ABCs. Notably, $\mathcal{F}^{\text{CLIM}}$ is derived from a 10-year long CROCO run forced by monthly climatological fields (CROCO^{CLIM}, see Table 1) and consists of 5 ensemble simulations in which CROCO SST forces WRF.

In the Supplementary Material, we compare the outputs of CROCO^{INTER}, $\mathcal{F}^{\text{CLIM}}$, and $\mathcal{F}^{\text{INTER}}$ with available observations, focusing on the quantities that control the ocean dynamics in the eastern equatorial sector and along the coast of southwestern Africa. Despite a slightly too diffuse thermocline, the forced ocean model has a realistic mean state that controls the modal structures and characteristics of the equatorial and coastal waves (see Supplementary Material S2). The associated WRF momentum and heat fluxes are in fair agreement with the ERA5 fields, but the surface solar radiation is underestimated. The interannual variability of SST, sea level, and surface winds is in very good agreement with remotely sensed observations, but with a notable reduction in the amplitude of the 2021 Atlantic Niño event (see Supplementary Material S3).

$\mathcal{F}^{\text{INTER}}$ is then declined into 2 sensitivity experiments (Table 1). First, \mathcal{F}^{MEM} differs from $\mathcal{F}^{\text{CLIM}}$ by its initial conditions on January 1, 2021, which come from $\mathcal{F}^{\text{INTER}}$. The difference between \mathcal{F}^{MEM} and $\mathcal{F}^{\text{CLIM}}$ allows to isolate the dynamics associated with the long-term ocean memory associated with the free propagating waves forced before 2021 (Sect. 4.2). In the $\mathcal{F}^{\text{CLIM-O}}$ sensitivity experiment, CROCO surface forcing is climatological, while WRF ABCs are interannual. Compared to $\mathcal{F}^{\text{INTER}}$ and $\mathcal{F}^{\text{CLIM}}$, this experiment will allow to disentangle the atmospheric response to the surface warming associated with the 2021 Atlantic and Benguela Niños from the effects of the interannual atmospheric forcing of the ABCs. This will be done in Sect. 3.

2.3 CROCO-WRF coupled simulations

We run a set of fully coupled CROCO-WRF simulations (Table 2), that will be analyzed in Sect. 4. Similar to the

Table 2 Set of coupled model experiments: Name of the experiment, design of the coupled experiment, period of the simulations, origin of CROCO restart, area of forcing/coupling, and WRF Atmospheric Boundary Conditions (ABCs, include or not interannual frequencies)

NAME	Design	Period	Restart	CROCO forcing/coupling area	WRF ABCs
\mathcal{C}^{CR}	CROCO \Leftrightarrow WRF	2021	CROCO ^{INTER-2020}	Coupled everywhere	Interannual
\mathcal{C}^{MEM}	CROCO \Leftrightarrow WRF	2021	CROCO ^{INTER-2020}	Coupled everywhere	No interannual
\mathcal{C}^{NW}	CROCO \Leftrightarrow WRF	2021	CROCO ^{INTER-2020}	Coupled everywhere	Interannual NW
$\mathcal{C}^{\text{SOUTH}}$	CROCO \Leftrightarrow WRF	2021	CROCO ^{INTER-2020}	Coupled everywhere	Interannual SOUTH
$\mathcal{C}^{\text{SOUTH_noBÑ}}$	CROCO \Leftrightarrow WRF	2021	CROCO ^{INTER-2020}	$\mathcal{C}^{\text{CLIM}}$ SST in the Benguela, coupled elsewhere	Interannual SOUTH
$\mathcal{C}^{\text{CLIM}}$	CROCO \Leftrightarrow WRF	2021	CROCO ^{CLIM-2020}	Coupled everywhere	No interannual

forced experiments (\mathcal{F}), the coupled simulations (\mathcal{C}) consist of 5 ensemble simulations that are spawned from CROCO^{INTER} or CROCO^{CLIM} on January 1, 2020 and are coupled with WRF only during the year 2021.

We first performed an interannual control run experiment (\mathcal{C}^{CR} , see Table 2), which starts from the same initial condition as $\mathcal{F}^{\text{INTER}}$ and in which the ABCs are interannual. The anomalies are estimated relative to a climatological sensitivity experiment ($\mathcal{C}^{\text{CLIM}}$) that resembles $\mathcal{F}^{\text{CLIM}}$ except that it is fully coupled in 2021.

We have examined the mean state and the interannual variability in the coupled context (see the Supplementary Materials). The results show that it takes less than 3 months for CROCO to adjust to the WRF air–sea fluxes, i.e. before the onset of the 2021 Atlantic and Benguela Niños. $\mathcal{C}^{\text{CLIM}}$ equatorial thermocline is too deep and diffuse compared to the forced simulations, resulting in a reduced Bjerknes feedback and smaller SST anomalies in the eastern equatorial Atlantic. Despite this amplitude bias, the coupled model is able to simulate the 2021 Atlantic Niño with a timing in relatively good agreement with the observations. The observed features of the 2021 Benguela Niño are also realistically captured by the coupled model, with magnitude and timing in agreement with the observations.

The overall good agreement between our key simulations and the observations implies that the equatorial and coastal ocean dynamics are adequately simulated by our model configuration. We thus performed sensitivity experiments on the origin of the triggering of the 2021 Atlantic and Benguela Niño events. Using interannual initial conditions from $\mathcal{F}^{\text{INTER}}$ and ABCs in which the interannual variability has been removed, \mathcal{C}^{MEM} (Table 2) allows us to test whether the triggering of the warm events is related to external conditions or, on the contrary, comes from the long-term ocean memory contained in the initial conditions, which may contain some variability that can later be amplified by the ocean–atmosphere coupling. The \mathcal{C}^{NW} solution allows to examine the role of any forcing coming from the Pacific basin, while $\mathcal{C}^{\text{SOUTH}}$ focuses on the effects of the atmospheric southern boundary fluxes. In $\mathcal{C}^{\text{SOUTH_noBÑ}}$, the atmospheric model cannot see the interannual SST anomalies along the African coast, south of 9° S, which allows to test the effects of coastal SST anomalies on the equatorial dynamics. These simulations are further detailed and analyzed in Sect. 4.

2.4 Interannual anomalies and key regions

Interannual variability is estimated as in Bachèlery et al. (2016). First, monthly anomalies are computed by estimating monthly means and subtracting the monthly climatological mean state. Subseasonal fluctuations are then removed using a 1–2–1 running weighted average and finally the time series are reinterpolated to their original temporal resolution using cubic splines.

For the long CROCO^{INTER} simulation, the time series are first linearly detrended and the monthly anomalies are estimated relative to the 2012–2021 monthly climatology. For the 2021 forced (family \mathcal{F} , see Table 1) and coupled (family \mathcal{C} , see Table 2) simulation sets, the climatological mean state is estimated using the sensitivity climatological simulations $\mathcal{F}^{\text{CLIM}}$ and $\mathcal{C}^{\text{CLIM}}$, respectively. Ocean atmosphere climatological model forcings are calculated over the period 2012–2021. The choice of this 10-year long period is a compromise between (1) the need to estimate a robust mean state that is not overly biased by exceptionally warm or cold years, and (2) the constraint that this mean state must be short enough to accurately represent the recent period over which the 2021 events developed and not average interdecadal variability over too long a period.

In the following, we will mainly analyze the interannual variability of the ocean (temperature, sea-level, mixed-layer depth) and the atmosphere (surface wind and wind-stress, and SLP) in 2021. We will focus on the dynamics along the equatorial waveguide (within the 3° S–3° N equatorial band) and in the ATL3 box ([20° W–0° E; 3° S–3° N], Zebiak (1993), see Fig. 1) and in the 2°-width coastal margin along West Africa and in the CABA box (20° S–10° S, Illig et al. (2020), see Fig. 1).

3 Forced dynamics of the 2021 Atlantic and Benguela Niño events

In this section, we describe the ocean dynamics at the origin of the interannual anomalies observed in the tropical Atlantic in 2021, and the associated atmospheric response. Our analyses are based on the ensemble mean of the realistic and sensitivity experiments carried out in a forced context and described in Sect. 2.2 (Table 1).

3.1 The realistic forced experiment

Figure 2 shows the anomalous surface and subsurface conditions during the 2021 Atlantic and Benguela Niño events as simulated by $\mathcal{F}^{\text{INTER}}$. Figure 2a, c focuses on the equatorial region, while Fig. 2b, d concentrates on the coastal band off West Africa. The forced model realistically simulates the observed features of these extreme events (see Fig. S5 in the Supplementary Materials) and both events show consistent signals in terms of wind stress, SLA, and temperature anomalies.

The Western-Central Equatorial Atlantic (WCEA) experiences a relaxation of the trade winds, starting in April 2021, which persists after October 2021 (Fig. 2a). The maximum zonal wind stress anomalies occur in June 2021 ($+1.7 \times 10^{-2}$ N/m² in WCEA) and force eastward-propagating downwelling EKW. The latter imprint the sea level and the thermocline depth in the eastern basin, with an SLA rise of 3.9 cm and a deepening of the thermocline of more than 5 m in ATL3 (Fig. 2c). The positive SLA anomalies reach the African boundary by the end of May 2021. The associated changes in the vertical and horizontal currents induce temperature anomalies that are maximum in mid-June in the vicinity of the thermocline ($+1.7$ °C at 45 m depth, see Fig. 2c), where the vertical temperature gradients are maximum. In ATL3, the SST anomalies lag behind the subsurface anomalies by 3 weeks. They peak in early July 2021 ($+0.9$ °C), when the thermocline and the mixed layer are close together. The SST anomalies persist throughout the boreal summer and fall (Fig. 2a), associated with negative net surface heat flux anomalies (not shown). This warming can be qualified as a strong Atlantic Niño because the SSTA averaged in ATL3 exceeds 1.5 times the standard deviation of the CROCO^{INTER} SSTA (STD=0.31 °C) for 3 consecutive months (June–August). From June onwards, an anomalous converging circulation develops over the warm event (Hu and Huang 2007; Illig et al. 2020), with westerly wind stress anomalies in the far eastern basin.

Along the coast of West Africa, the 2021 Benguela Niño event begins before the onset of the Atlantic Niño. Positive

SSTA starts as early as January 2021 in the Angola Benguela Frontal Zone and in March 2021 along the coast of South Africa (Fig. 2b). The warming then intensifies and spreads along the coast of Namibia, concomitant with strong poleward wind stress anomalies favorable for anomalous downwelling conditions and reduced evaporation. South of 15° S, the maximum warming exceeds 2.5 °C at 17.5° S in early May, accompanied by positive SLA greater than 3 cm. In the CABA domain (Fig. 2d), the thermocline is shallower than in the equatorial region (~25 m depth) and is closer to the base of the mixed layer. As a result, the surface warming from March to August is simultaneous and as intense as the subsurface warming. It peaks in mid-May 2021 ($+1.75$ °C), 6 days before the SLA maximum ($+3.6$ cm). In the northern half of the coastal region, the warming is slightly less intense and peaks later, in June 2021. It is accompanied by a coherent coastal SLA rise of more than 4 cm. North of the Congo estuary, the SLA exceeds 6 cm and its timing is consistent with the arrival of the downwelling EKW at the Gabonese coast. Notably, the anomalous surface wind circulation north of 15° S is contrasting from the southern half of the domain, characterized by moderate equatorward wind stress anomalies. Following Imbol Koungue et al. (2019), this warm event can be qualified as an extreme Benguela Niño because the 1°-wide coastal SSTA exceeds the 2012–2021 standard deviation of the CROCO^{INTER} SSTA from April to July 2021 in their three coastal domains (southern Angola (10° S–15° S, STD=0.44 °C), Angola Benguela Front (15° S–19° S, STD=0.55 °C), and northern Namibia (19° S–24° S, STD=0.42 °C)).

The overall sequence remains in good agreement with the dynamics described in Illig et al. (2020). The coastal event starts and peaks before the equatorial warming. In the equatorial band, the sequence of interannual anomalies is consistent with the propagation of wind-driven equatorial downwelling waves forced by a relaxation of the trade winds in the WCEA. They imprint the sea level and the SST in the east and reach the African boundary by the end of May 2021. Along the African coast, the warming is associated with both local and remote forcing. South of 15° S, southward coastal wind anomalies reduce the coastal upwelling and the evaporation, while in the northern coastal region, equatorially forced CTWs induce warm SSTA, despite the equatorward upwelling-favorable coastal winds.

3.2 The basin-scale atmospheric conditions

We further examine the anomalous atmospheric circulation that leads to the warm events. Figure 3 shows the map of ERA5 interannual anomalies of SLP (colors) and 10-m winds (arrows) in March and May 2021. The full series of maps from February to July 2021 is shown in the

FRC Experiment – Control Run

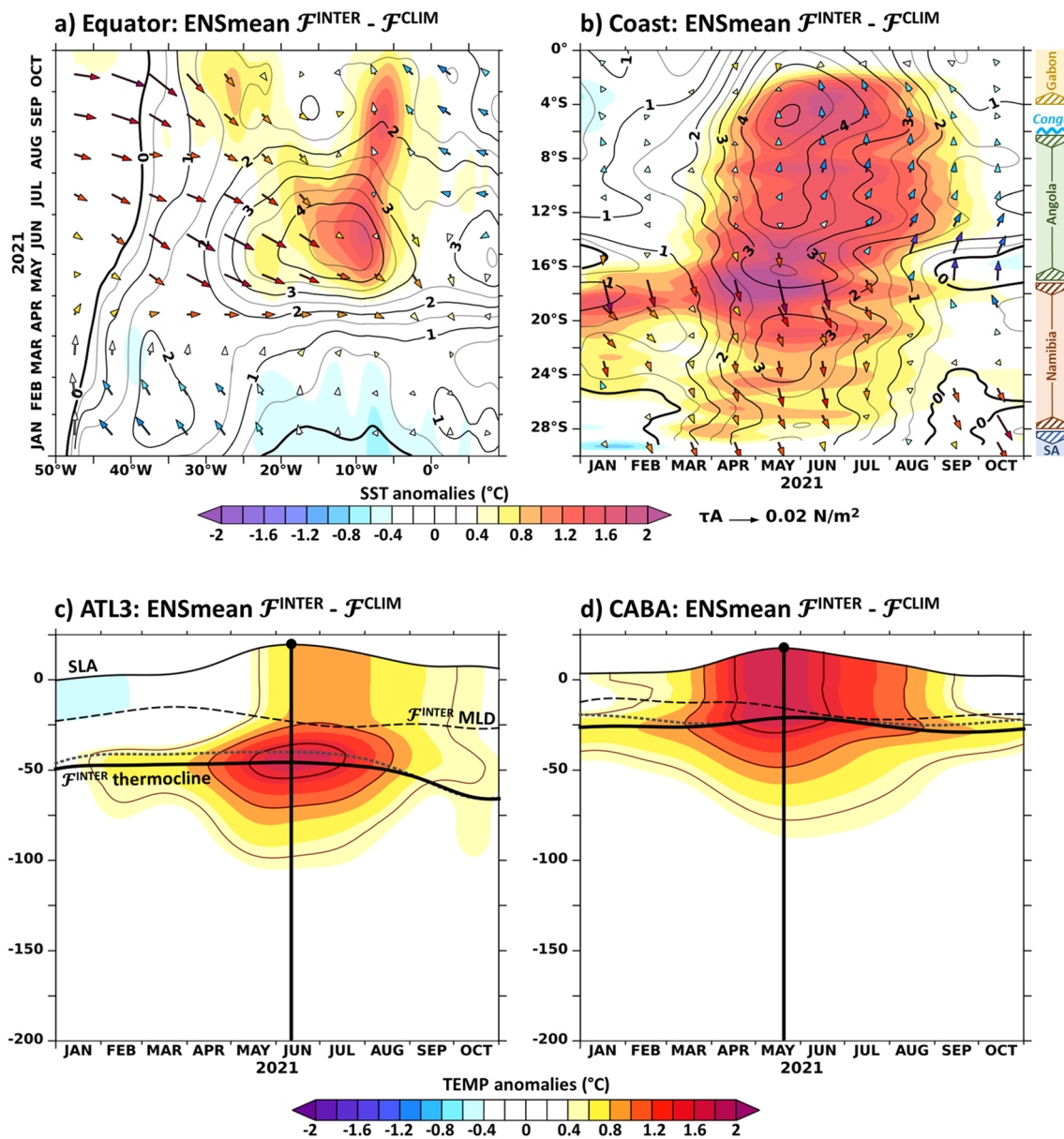


Fig. 2 The 2021 Atlantic and Benguela Niño events simulated by the ensemble mean of our realistic forced experiment \mathcal{F}^{INTER} (see Table 1). **a** Hovmöller plot of CROCO SSTA (shading, °C), SLA (contours, cm), and WRF surface wind stress anomaly response (arrows, with colors representing the zonal amplitude, N/m^2) averaged within the 3° S–3° N equatorial band. **b** Same as panel a, but for the 2°-wide fringe along the African coast, with arrow colors indicating the meridional wind-stress amplitude. **c** Equatorial temperature anomalies averaged in the ATL3 box as a function of depth and time.

Exaggerated free surface variations denote the evolution of the SLA (SLA (in m) is multiplied by a factor of 500). The SLA peak is highlighted with a vertical line. The dashed line indicated the position of the mixed-layer depth. The thick black (thin dashed grey) line shows \mathcal{F}^{INTER} (\mathcal{F}^{CLIM}) thermocline position. **d** Same as c, but for the coastal interannual anomalies averaged in the CABA box. Interannual anomalies are computed relative to the forced climatological simulation \mathcal{F}^{CLIM} . The figure has been realized using the Ferret program (<http://ferret.pmel.noaa.gov/Ferret/>)

Supplementary Material (Fig. S6). Prior to the development of the Atlantic Niño event, the SLP is significantly weaker than the normal conditions, with negative SLP anomalies extending throughout our model domain, from 35–40° S

to 20° N. Important negative SLP anomalies are observed south of 20° S and extend to the coast of Africa. Maximum values are located east of the core of the SAA at ~28° S. The strength of the SAA is weakened, and its position is

Basin-scale atmospheric conditions

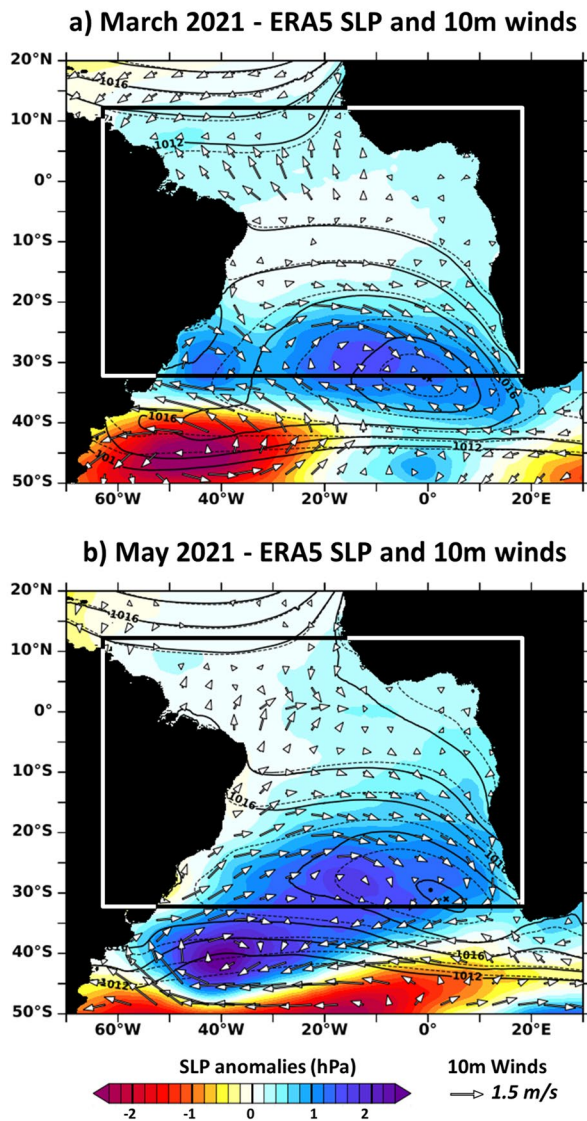


Fig. 3 Basin-scale atmospheric conditions in the tropical Atlantic in **a** March 2021 and **b** May 2021. Sea Level Pressure (SLP, colors, hPa) and 10-m winds (arrows, m/s) interannual anomalies. SLP is shown in solid contours, with the maximum SLP of the South Atlantic Anticyclone (SAA, 1020.2 hPa) marked with a cross, as compared to the normal conditions [dashed contours, with a dot indicating the maximum SLP of the SAA (1021.4 hPa)]. The rectangle delineates our WRF atmospheric model domain. The full series of maps from February to July 2021 is shown in Fig. S6 of the Supplementary Material. The figure has been realized using the Ferret program (<http://ferret.pmel.noaa.gov/Ferret/>)

closer to the coast of South-Africa, as shown by the SLP isobars (plain contours) compared to the normal conditions (dashed contours). This pattern is quite stable: it develops in March 2021 and persists until June 2021. The associated surface atmospheric circulation is dominated by anomalous geostrophic motions, portraying strong cyclonic anomalous

winds near the core of the SAA and affecting the coastal winds off southwest Africa. Off Angola, Namibia, and South Africa, northerly wind anomalies induce the early coastal warming starting in January in the Angola Benguela Frontal Zone and in March 2021 off the south African coast (Fig. 2b), presumably through local processes (downwelling and reduced evaporation). From February to April 2021, in the equatorial band, WCEA surface wind stress anomalies are northwestward and the relaxation of the trade winds does not develop until in May 2021. A few weeks later, positive SSTA develops in the east-equatorial Atlantic, associated with the remotely forced downwelling EKW (Fig. 2a). The subsequent downwelling CTWs can then trigger the coastal warming north of 16° S and can amplify the warming in the southern coastal domain.

These large-scale atmospheric conditions are consistent with the sequence proposed by Illig et al. (2020), but the relationship between the relaxation of the WCEA trade winds and the position and intensity of the SAA is not straightforward in Fig. 3, as compared to Illig et al. (2020) (their Fig. 13). The weakening of the SLP south of 20° S is indeed well established since March 2021 (Fig. 3a), while the eastward equatorial zonal wind stress anomalies are observed only since May 2021 (Fig. 3b). Before that, the northwesterly WCEA wind anomalies seem to be driven by the positive SSTA in the north tropical Atlantic (WMO-No 1300 2022). Thus, the triggering of the 2021 Atlantic Niño requires further investigation.

3.3 The atmospheric response to boundary-forcing and SST

As a preliminary analysis, we performed a forced sensitivity experiment ($\mathcal{F}^{\text{CLIM-O}}$, see Table 1) in which the CROCO surface forcing is climatological, while the WRF ABCs remain interannual. Assuming some linearity, the difference between $\mathcal{F}^{\text{CLIM-O}}$ and $\mathcal{F}^{\text{CLIM}}$ (Fig. 4ab) shows the atmospheric response only to the interannual atmospheric fluxes at WRF ABCs, while the difference between $\mathcal{F}^{\text{INTER}}$ and $\mathcal{F}^{\text{CLIM-O}}$ (Fig. 4c, d) results only from the surface warming associated with the 2021 Atlantic and Benguela Niños simulated by $\mathcal{F}^{\text{INTER}}$. In the equatorial band, the results show that both the boundary and SSTA forcings contribute to the relaxation of the trade winds in the WCEA (Fig. 4a, c). The atmospheric boundary forcing, presumably from the west (63.5° W), drives equatorial positive zonal wind stress anomalies from April 2021 to October 2021, confined to the WCEA (Fig. 4a). The SSTA forcing also triggers positive zonal wind stress anomalies starting in the eastern basin as early as January 2021 and slowly spreading westward to occupy the entire equatorial band by April 2021 (Fig. 4c). In May and June 2021, there is a noticeable increase in the wind stress anomalies in the west, likely due to the modification

FRC Experiments – Effects of the Atmospheric Response

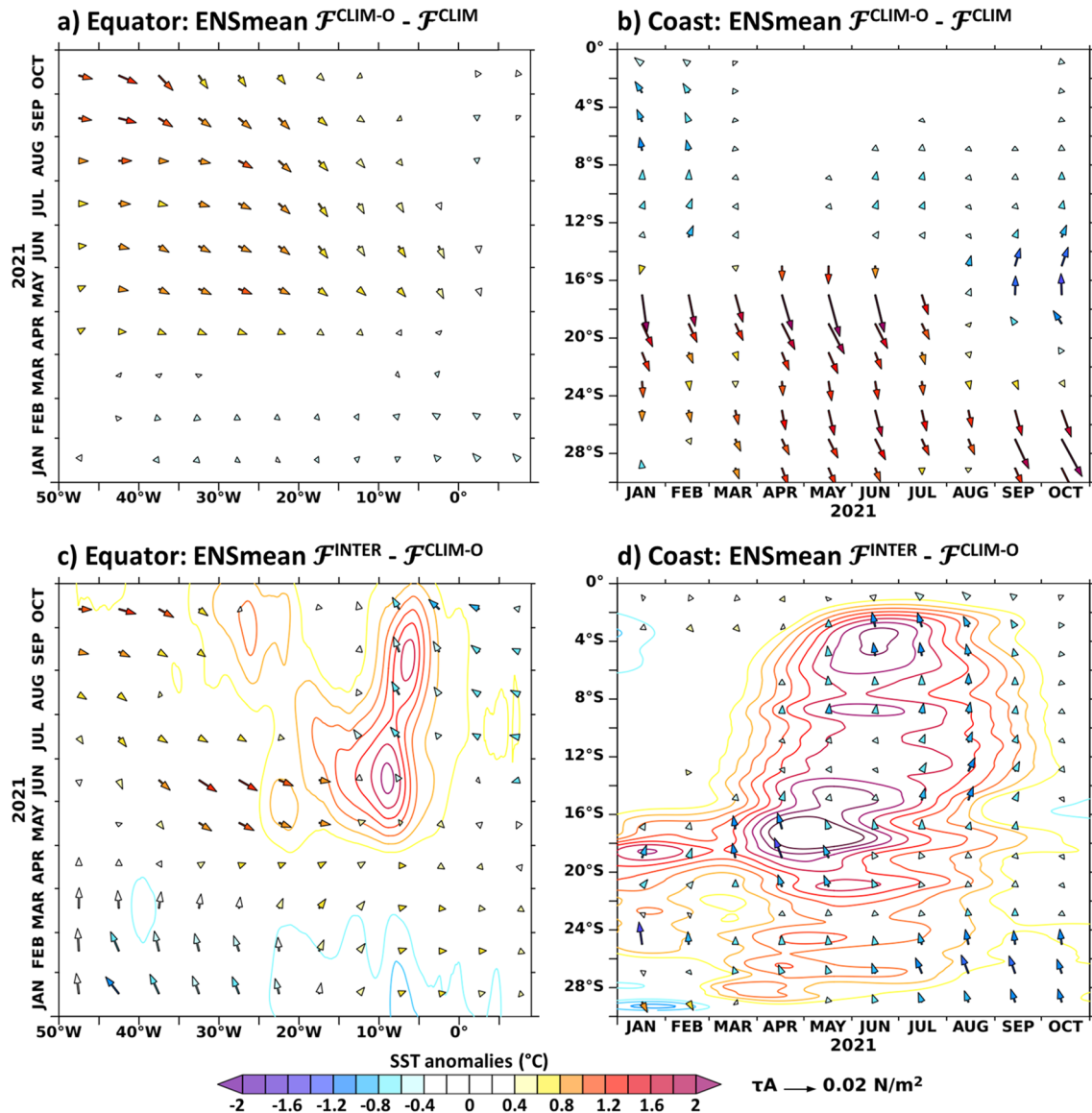


Fig. 4 Atmospheric response in the equatorial and coastal bands. **a, b** Effect of the Atmospheric Boundary Conditions: same as Fig. 2a, b, but for the differences between $\mathcal{F}^{\text{CLIM-O}}$ and $\mathcal{F}^{\text{CLIM}}$. SSTA and SLA differences are zero because the ocean components of $\mathcal{F}^{\text{CLIM}}$ and $\mathcal{F}^{\text{CLIM-O}}$ are identical (see Table 1). **c, d** Effect of the SSTA: same

as Fig. 2a, b, but for the differences between $\mathcal{F}^{\text{INTER}}$ and $\mathcal{F}^{\text{CLIM-O}}$. Colored contours correspond to $\mathcal{F}^{\text{INTER}}$ SSTA shown in Fig. 2a, b. The figure has been realized using the Ferret program (<http://ferret.pmel.noaa.gov/Ferret/>)

of the Atlantic Walker circulation associated with the 2021 Atlantic Niño. From June onwards, anomalous ascending motions associated with the eastern equatorial warm event trigger a converging surface anomalous circulation, associated with negative zonal wind stress anomalies in the far eastern basin.

The analysis of the sensitivity experiments along the African coast further shows that from January to August 2021, the poleward coastal wind stress anomalies south of 15° S

(Fig. 2b) that initiate the 2021 Benguela Niño are controlled by the interannual fluxes prescribed at the atmospheric model boundaries (Fig. 4b), most likely from the south (32° S). In contrast, in the northern coastal region, ABCs drives wind stress anomalies with the opposite direction, favorable to cold conditions. Meanwhile, the warm SSTA in the tropical Atlantic triggers equatorward coastal wind stress anomalies starting south of 15° S in January–February 2021 and extending over all of West Africa from April 2021 (Fig. 4d).

This anomalous circulation is concomitant with a deeper and more unstable Marine Atmospheric Boundary Layer (MABL) associated with the warmer coastal margin in $\mathcal{F}^{\text{INTER}}$. In the CABA region and on average between April and July 2021, the MABL in $\mathcal{F}^{\text{INTER}}$ is indeed 50 m higher than in $\mathcal{F}^{\text{CLIM-O}}$, and local anomalies of +100 m are exceeded north of 10° S in May–June 2021. The coastal northerly wind stress anomalies correspond to enhanced coastal mean surface winds, which in turn can favor increased upwelling and evaporation, i.e. a negative feedback. This anomalous circulation is later reinforced by the air–sea interaction in the Gulf of Guinea, i.e. by the equatorward coastal winds associated with the southeastern branch of the converging circulation that develops over the equatorial warming (Illig et al. 2020).

The 2021 Benguela Niño appears to be initiated by the atmospheric circulation south of 30° S, but so far it is not clear which process initiates the wind anomalies that lead to the equatorial warming via downwelling EKW propagation. From the results in Fig. 4a and Fig. 4c, we conclude that both the atmospheric fluxes at the WRF boundaries and the SSTA contribute to the relaxation of the equatorial trade winds. However, at this stage it is not possible to disentangle the atmospheric response to the eastern equatorial Atlantic SSTA from that associated with the coastal warming. This needs to be addressed in a coupled context, which is done in the following section.

4 On the triggering of the 2021 Atlantic and Benguela Niño events

In this section, we focus on the causes that led to the development of the 2021 Atlantic and Benguela Niño events. This is done in a coupled context, and we analyze the ensemble mean of the experiments described in Sect. 2.3 (Table 2). The coupled control run experiment (\mathcal{C}^{CR}) provides a benchmark for the analysis of the sensitivity experiments designed to assess the contribution of the long-term memory of the ocean, the atmospheric fluxes from the Pacific and from the South, and the air–sea interactions within the tropical Atlantic to the phenology of the 2021 extreme events.

4.1 The coupled control run experiment

Figure 5 shows the \mathcal{C}^{CR} 2021 anomalous conditions at the air–sea interface and in the subsurface, similar to Fig. 2. The coupled model manages to simulate the salient features of the 2021 Atlantic and Benguela Niño events, with a timing in good agreement with the observations (see Sect. S3 and Fig. S5 in the Supplementary Materials) and the interannual forced experiment (Fig. 2), except for the surface signature of the Atlantic Niño. In

the equatorial Atlantic, the year 2021 begins with moderately cold surface conditions that slowly warm during the first 3 months (Fig. 5a). In April, the relaxation of the trade winds forces a downwelling EKW, which is easily detected by its SLA imprint (red arrow in Fig. 5a). It crosses the basin in 1.5 months (~ 1.7 m/s) and reaches the eastern boundary on May 27, at the same time as in the forced experiment (Fig. 2a). Along its path, it deepens the thermocline and induces temperature anomalies that are amplified by the reflected westward-propagating equatorial downwelling Rossby wave (red arrow in Fig. 5a). In the eastern equatorial Atlantic (ATL3 region), the warming reaches its pinnacle in early June 2021 (+1.86 °C at 65 m), near the thermocline (Fig. 5c). However, the thermocline in the coupled simulation is significantly deeper than in the forced simulations (+20 m in May–June 2021 in ATL3). Despite the deeper mixed layer, the subsurface anomalies, which are slightly larger in \mathcal{C}^{CR} than in $\mathcal{F}^{\text{INTER}}$, have more difficulty reaching the surface and they also take slightly more time to imprint the SST (36 days) than in the forced run (24 days). A reduced surface warming is also detrimental in terms of the atmospheric response and the intensity of the Bjerknes positive feedback. As a result, compared to $\mathcal{F}^{\text{INTER}}$, the amplitude of the maximum zonal wind stress anomalies in the WCEA ($+0.81 \times 10^{-2}$ N/m²) is reached one month earlier (on May 8), and the maximum SSTA in ATL3 barely exceeds 0.5 °C on July 11. Equatorial stratification is also weaker in \mathcal{C}^{CR} than in $\mathcal{F}^{\text{INTER}}$ (see Sect. S2 in the Supplementary Materials), favoring low-order baroclinic modes and vertical mixing. This explains the amplitude and vertical extent of the subsurface warming and the associated SLA fluctuations: despite the reduced momentum forcing, both remain in the same order of magnitude as in $\mathcal{F}^{\text{INTER}}$ (Fig. 2c). It is important to recall here that the WRF ABCs are identical in \mathcal{C}^{CR} and in $\mathcal{F}^{\text{INTER}}$, highlighting the importance of the air–sea interactions when analyzing the difference between \mathcal{C}^{CR} and $\mathcal{F}^{\text{INTER}}$. In particular, from July onwards, the surface wind-stress anomalies are much smaller in \mathcal{C}^{CR} as compared to $\mathcal{F}^{\text{INTER}}$ (Fig. 5a), and the converging circulation barely forms over the warm equatorial event. This impacts the coastal dynamics off West Africa, in particular north of 15° S. There, the ocean connection to the equatorial variability remains strong, showing a coherent southward-propagating coastal SLA with an amplitude greater than 5 cm (Fig. 5b). However, as in the equatorial band, the deeper (+25 m in the coastal band between 0° N and 10° S) and less stratified thermocline prevents a strong surface signature (SSTA < 0.7 °C), despite a slightly more intense subsurface warming in \mathcal{C}^{CR} (> 2 °C at 40 m in early June 2021) than in $\mathcal{F}^{\text{INTER}}$. The associated equatorward wind anomalies are consequently reduced and delayed into the boreal summer. In the southern half of the coastal domain,

CPL Experiment – Control Run

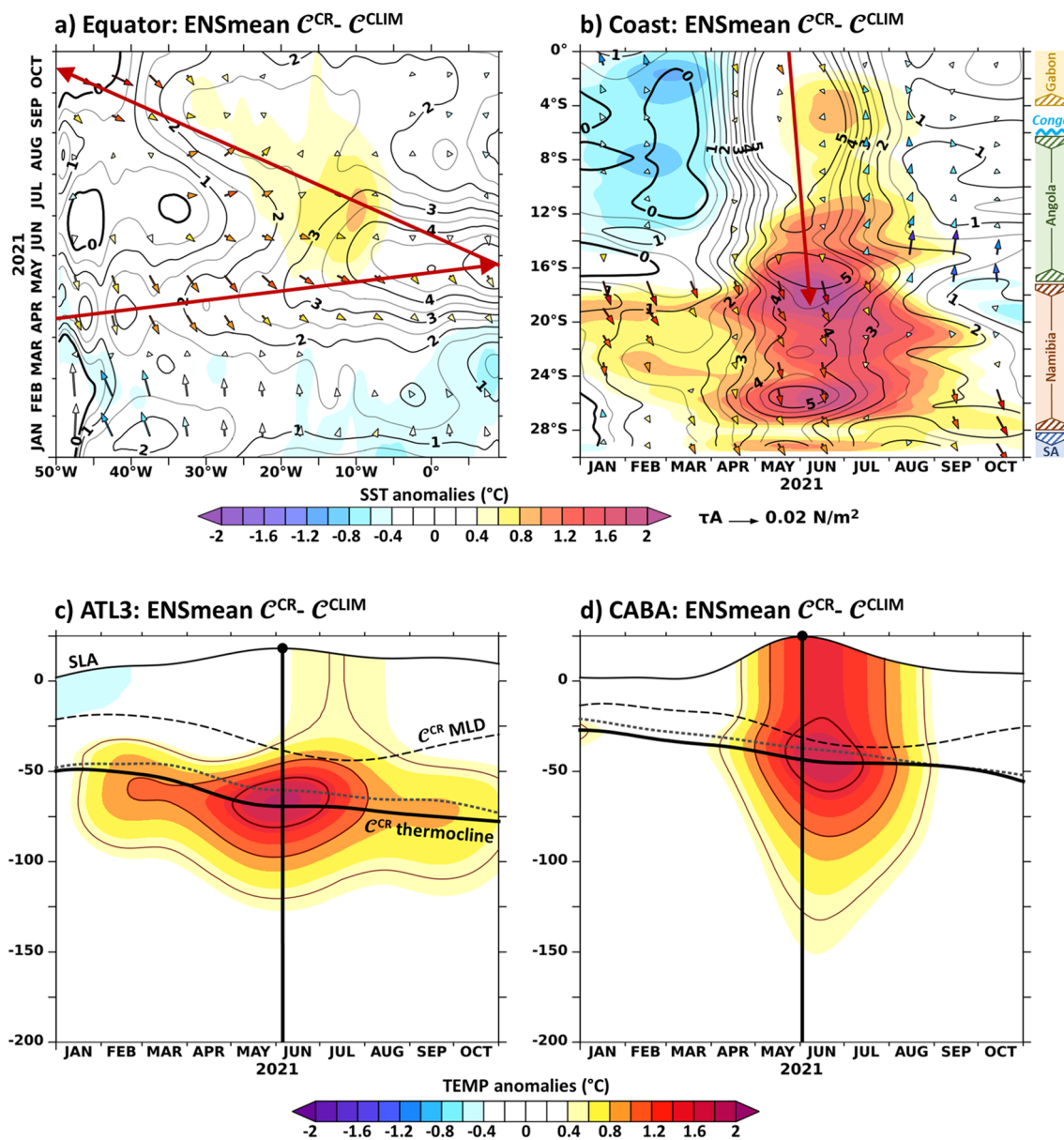


Fig. 5 Results of the control-run coupled experiment C^{CR} . Same as Fig. 2, but for the ensemble mean of C^{CR} simulations. Interannual anomalies are estimated relative to the coupled climatological simulation C^{CLIM} . In the upper panels, red arrows show the equatorial (panel

a) and coastal (panel b) wave propagations described in Sect. 4.1. The figure has been realized using the Ferret program (<http://ferret.pmel.noaa.gov/Ferret/>)

the coastal warming is stronger and delayed by one month than in \mathcal{F}^{INTER} (Fig. 2b): on average in the coastal fringe from 20° S to 30° S, the SSTA maximum exceed 1.3 °C in the end of June 2021, while in \mathcal{F}^{INTER} it is less than 0.9 °C at the end of May 2021. This may be due to the modal contribution of the equatorial forcing, with the deeper stratification favoring less-dissipative low-order modes, prone to a stronger and more distant connection with the warm

equatorial variability (Illig and Bachèlery 2019). South of 15° S, the poleward surface stress anomalies in C^{CR} are in very good agreement with the forced experiment (Fig. 5b), with a somewhat slightly smaller amplitude. This can be attributed to the increased negative feedback associated with the increased coastal surface warming and the deeper overlying MABL in C^{CR} . Consistent with the observations (see Fig. S5b in the Supplementary Materials), the overall

coastal pattern of North/South remotely/locally-forced positive coastal SLA slightly reveals the banana-shaped pattern described in Bachèlery et al. (2020).

In conclusion, the coupled model captures the variability associated with the 2021 Atlantic and Benguela Niño events, especially in the subsurface. However, the reduced SSTA signature north of 15° S, mainly due to the biases in the mean state of the coupled simulations, will affect the air–sea interactions. This has to be taken into account when analyzing the coupled sensitivity experiments.

4.2 External or internal triggering

In this section, we analyze the effects of the long-term ocean memory associated with free propagating waves forced before 2021. We want to test whether the seeds of the 2021 tropical Atlantic warming were planted before 2021 and are then amplified by the ocean–atmosphere coupling. To test this hypothesis, we performed a sensitivity experiment, C^{MEM} (Table 2), in which the coupled model is initiated with the same ocean and atmosphere conditions as in C^{CR} . Contrary to C^{CR} , there is no interannual external forcing in C^{MEM} because the interannual fluxes have been filtered-out at WRF ABCs. The results shown in Fig. 6 need to be compared with our coupled control experiment (C^{CR} , see Fig. 5).

The 2021 interannual variability in C^{MEM} is characterized by a downwelling EKW propagation that crosses the basin in January 2021 that can be seen on the clear eastward-propagating pattern in the positive SLA larger than 1 cm (see dashed arrow in Fig. 6a). This wave most likely originates from the reflection of an equatorial downwelling Rossby wave at the Brazilian coast. It warms the January moderately cold surface conditions and in March the equatorial Atlantic shows neutral conditions. This wave reaches the coast of Gabon in early February 2021, where a part of its energy is transferred back towards the center of the basin as a westward-propagating equatorial Rossby wave. A significant part of the downwelling wave energy is transmitted along the coast of West Africa as a downwelling CTW, imprinting the coastal SLA up to the Namibian coasts in March–April 2021 (dashed arrow in Fig. 6b). Along the way, these waves trigger moderate positive temperature anomalies in the eastern equatorial sector and along the African coast in the vicinity of the thermocline (Fig. 6c, d). In the ATL3 (CABA) region, the subsurface temperature anomalies do not exceed 1 °C (0.5 °C) in February (March–April) 2021. These anomalies are significantly smaller than those associated with the 2021 Atlantic and Benguela Niños in C^{CR} (Fig. 5c, d) and they do not spread to the surface layer, generating no further air–sea interactions. Note that we do indeed obtain a quasi-identical sequence of interannual fluctuations for the forced twin experiment (\mathcal{F}^{MEM} , see Table 1), in which CROCO is forced with climatological surface fluxes (not shown). Moreover,

the timing of C^{MEM} free propagations is not consistent with the observed interannual events (Fig. 5) as they affect the temperature and the SLA in the late boreal winter, i.e. more than 3 months before the actual peaks of the 2021 Atlantic and Benguela Niños.

In conclusion, the pre-2021 ocean variability is not the main cause of the development of the 2021 tropical Atlantic extreme events. However, it most likely has contributed to the preconditioning of the ocean with a warming of the surface layer during the first trimester of 2021, allowing neutral conditions to be reached in March. Note that we do not investigate the potential role of the Congo runoff on the dynamics of the 2021 extreme events, although it has been suggested to play a significant role in the development of the 2016 Benguela Niño (Lübbecke et al. 2019). In fact, the monthly flow of the Congo-Oubangui River in 2021 did not present any significant changes compared to the climatology, showing a near-to-below average (WMO No-1300 2022). Note also that C^{CR} captures the salient features of the 2021 interannual tropical Atlantic variability without interannual ocean boundary conditions (Sect. 2.1), which eliminates this forcing as a potential trigger for the 2021 interannual variability. Consequently, the external forcing prescribed at the atmospheric model boundaries must be the trigger for the 2021 Atlantic and Benguela Niño events. In the following sections, we disentangle the effects of the Pacific inflows from the southern forcing.

4.3 Influence of the Pacific Ocean

In this section, we focus on some potential atmospheric external forcings that could have triggered the changes in the position and intensity of the SAA in 2021. Of particular interest are the fluxes coming from the equatorial Pacific Ocean. Indeed, in 2021 the Pacific experienced moderate-strength La Niña conditions early in the year, which evolved into an ENSO-neutral state in June–July, and then returned back to a stronger La Niña situation from October onwards (WMO No-1300 2022; Li et al. 2022). As shown in Fig. 1, the eastern equatorial Pacific was colder than normal at the onset of the 2021 Atlantic Niño, which may have favored subsidence over the South American continent and triggered eastward surface wind anomalies in the western equatorial Atlantic, as was the case for the 1996 Atlantic Niño (Handoh and Bigg 2000; Illig et al. 2006). Positive SSTA were also observed in the eastern tropical North Atlantic in the first trimester of 2021 (WMO No-1300 2022), which also have the potential to influence the surface wind circulation in the WCEA (Illig and Dewitte 2006).

As shown in the ERA5 dataset (Fig. 7b), there was indeed an easterly wind flow in the spring of 2021 that entered the western boundary of our coupled model (at 62° W), which was confined to the equatorial waveguide ([5° S–5° N])

CPL response assoc/wth Ocean MEM

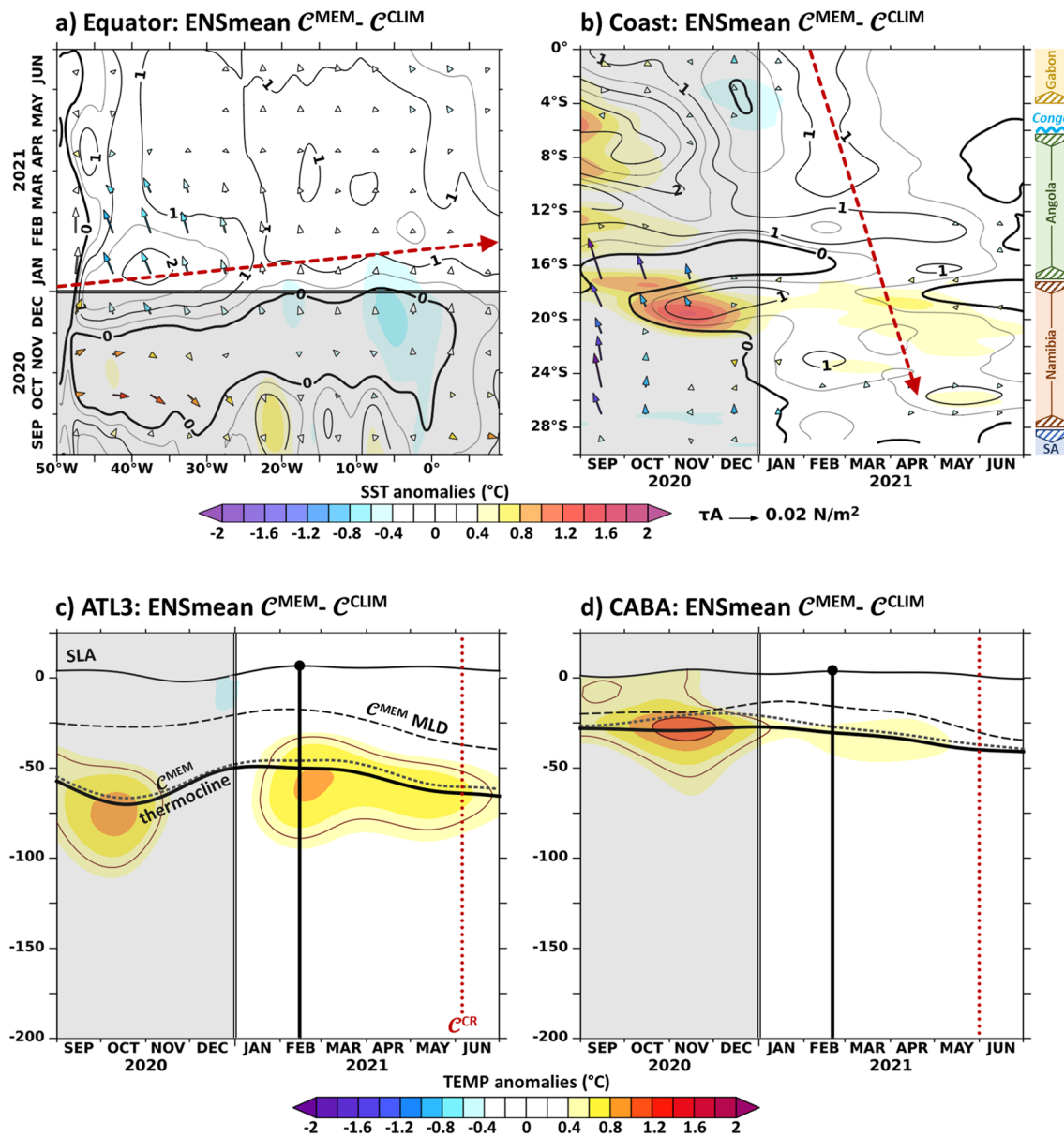


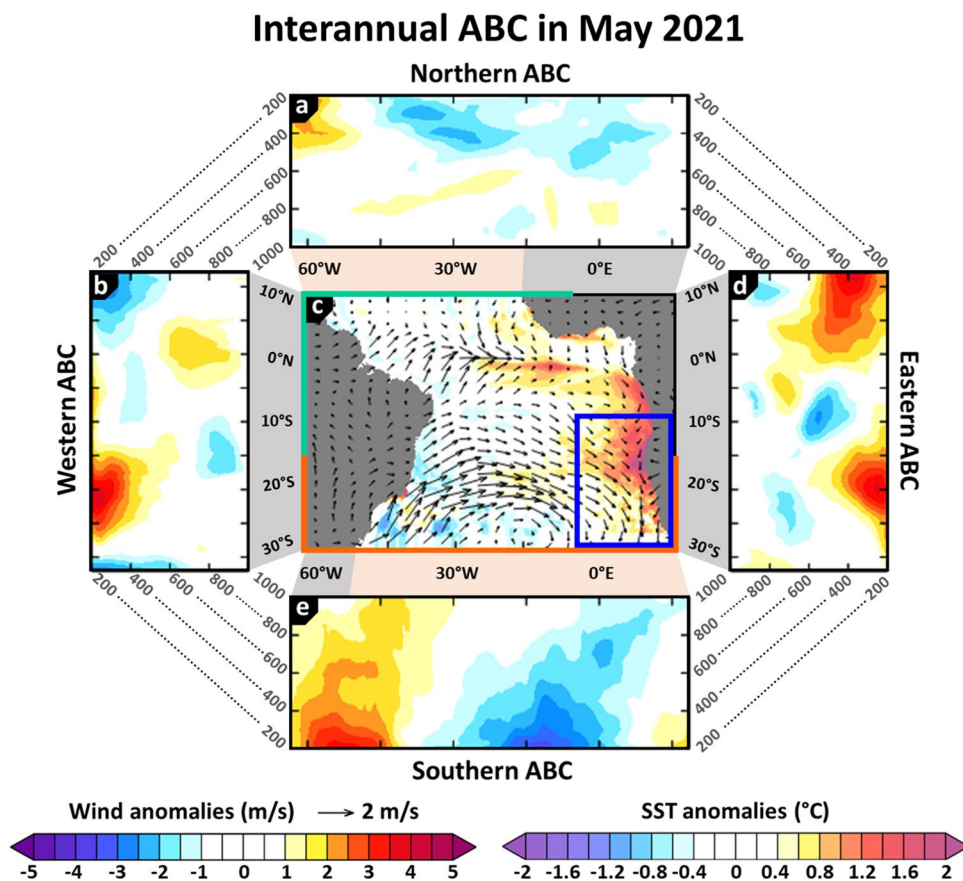
Fig. 6 Coupled response associated with the long-term ocean memory. Same as Fig. 5, but for the ensemble mean of the C^{MEM} simulations over the period Sep 2020–Jun 2021. The year 2020 has been grayed-out because it consists of the anomalies of the ensemble mean of the $CROCO^{INTER-2020}$ forced simulations (relative to $CROCO^{CLIM-2020}$, see Table 1). In the upper panels, red dashed

arrows show the equatorial (panel a) and coastal (panel b) wave propagations described in Sect. 4.2. In the lower panels, the vertical red dotted lines indicate the maximum SLA in C^{CR} (from Fig. 5c, d). The figure has been realized using the Ferret program (<http://ferret.pmel.noaa.gov/Ferret/>)

between the ground and 500 hPa. It started in April 2021 and lasted throughout the fall of 2021, with a maximum of 3 m/s in June 2021 (not shown). And we showed in Sect. 3.3 that the atmospheric response to the WRF ABCs has the potential to produce a relaxation of the Atlantic trade winds up to 0° W (Fig. 4a). At the northern boundary (12° N), a southward inflow occurred from March to May

2021, confined to the upper layers above 500 hPa. To assess the effects of this external forcing coming from the north and the west on the coupled interannual variability of the tropical Atlantic, we designed a sensitivity experiment C^{NW} (Table 2), in which the interannual variability of the WRF ABCs is restricted to the northwestern quadrant, from 15° S to 5° W (see the green boundary in Fig. 7c). Note that, to

Fig. 7 ERA5 atmospheric anomalous conditions at the boundaries of the WRF domain in May 2021. Anomalies are computed relative to the 2012–2021 monthly climatology. Upper (a) and lower (e) panels show the interannual meridional velocity anomalies (m/s) from 1000 to 200hPa. Positive values indicate a northward flow. Similarly, the left (b) and right (d) panels show the zonal velocity anomalies (m/s) with positive values for an eastward flow. The middle panel (c) shows ERA5 10 m-wind anomalies (arrows, m/s) overlaying $\mathcal{T}^{\text{INTER}}$ SST anomalies (shading, °C). Green, orange, blue contours refer to specific forcing regions of C^{NW} , C^{SOUTH} , and $C^{\text{SOUTH}_{\text{noBN}}}$ coupled sensitivity experiments described in Sect. 2.3 (see Table 2) and analyzed in Sect. 4. The figure has been realized using the Ferret program (<http://ferret.pmel.noaa.gov/Ferret/>)



reduce spurious wind gradients, a gradual (linear) transition zone of 5° width is appended to the south and east between the region where interannual ABCs are prescribed and the region where filtered fluxes are imposed. The interannual variability simulated by C^{NW} is shown in Fig. 8. Surprisingly, the results reveal that the interannual variability in C^{NW} shares more similarity with C^{MEM} free wave propagations (Fig. 6) than with our most realistic coupled simulation, C^{CR} (Fig. 5). The SLA fluctuations indeed portray a downwelling EKW propagation that crosses the basin very early in the year (Fig. 8a). Upon arrival at the African coast at the end of February 2021, it excites a poleward coastal propagation that propagates up to the South-African coasts (Fig. 8b). Compared to the C^{MEM} experiment, the downwelling waves in C^{NW} are more energetic, boosted by the inflow prescribed at the northwestern atmospheric boundaries. In the equatorial region, the SLA associated with the January–February downwelling wave exceeds 3.5 cm at the coast of Gabon, and it is even possible to follow its subsequent reflections into equatorial Rossby and then Kelvin waves (see dashed arrows in Fig. 8a). It is also nice to see the associated CTW propagation in the Fall of 2021 (Fig. 8b). However, the equatorial waves have a very limited signature in terms of SSTA (Fig. 8c) and remain free equatorial propagations. Along the African coast, the C^{NW} CTW is also more energetic than in

C^{MEM} (Fig. 8b) and, south of 10° S, the associated temperature anomalies imprint on the SSTA in the Boreal Spring of 2021 (Fig. 8d). However, the timing of the C^{NW} waves is not consistent with the C^{CR} 2021 dynamics. The C^{NW} subsurface equatorial warming in ATL3 peaks in February 2021, 3 months before the observed 2021 Atlantic Niño, and the coastal warming in CABA is also 2 months too early compared to in C^{CR} .

In conclusion, the inflow from the Pacific Ocean and the North tropical Atlantic does not succeed in triggering the 2021 Atlantic and Benguela Niño events. However, its coupled response, together with the wave sequence initiated before 2021, have definitely contributed to the warming of the equatorial thermocline layers from January to March 2021. In the following section, we examine the effects of the atmospheric fluxes entering and exiting the tropical Atlantic from the South (32° S).

4.4 Forcing from the South

At the southern boundary of our model domain in May 2021 (Fig. 7e), strong winds blew southward, confined near the African coast and extending from the sea surface up to the top of the troposphere. Concurring with Fig. 3, the southward anomalous winds started in March 2021

CPL response assoc/wth ATM NorthWestern fluxes

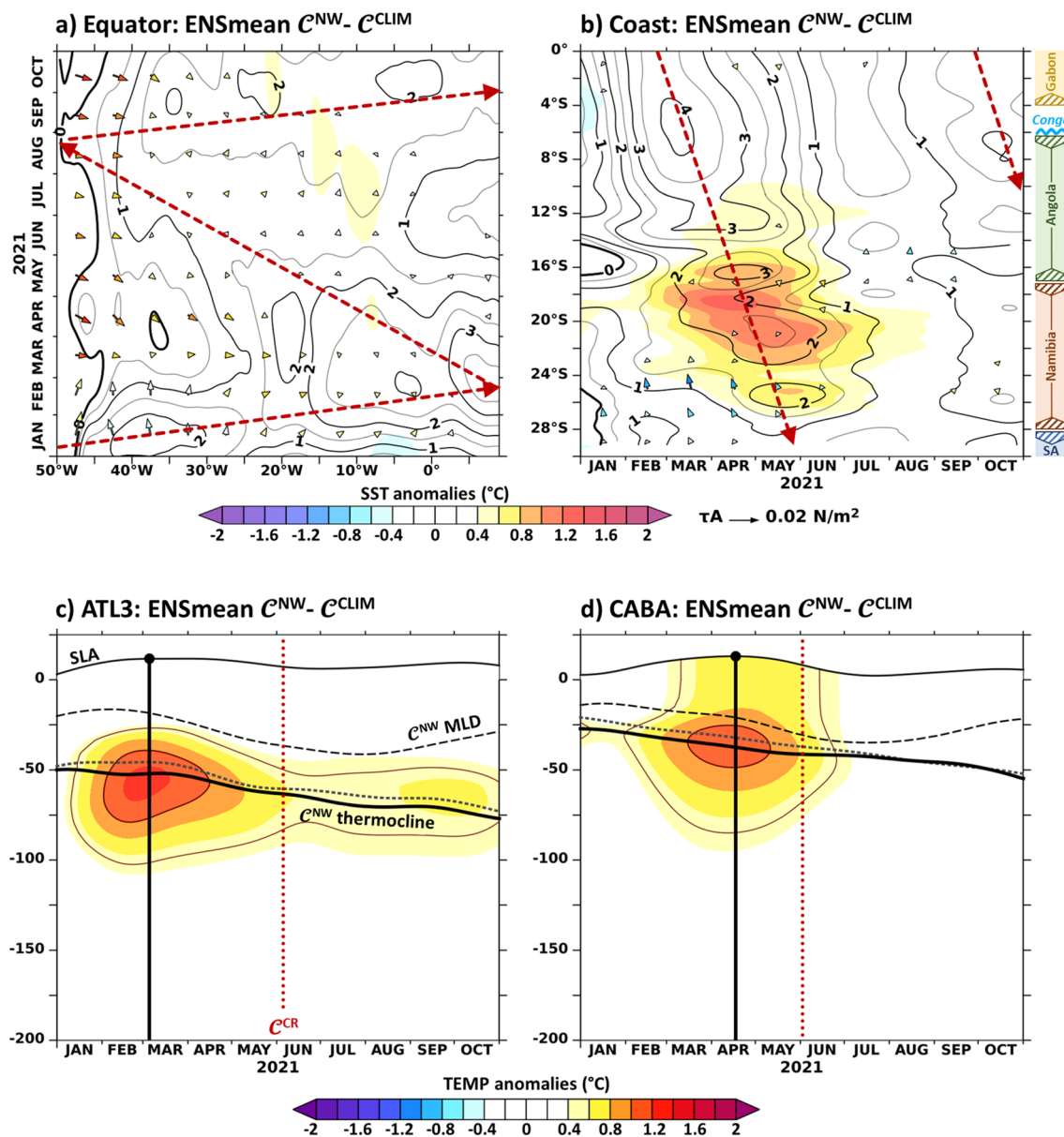


Fig. 8 Coupled response associated with northwestern atmospheric fluxes. Same as Fig. 5, but for the ensemble mean of the C^{NW} simulations. In the lower panels, the red vertical dotted lines indicate the maximum SLA in C^{CR} (from Fig. 5). In the upper panels, red dashed arrows show the equatorial (panel a) and coastal (panel b) wave

propagations described in Sect. 4.3. In the lower panels, the vertical red dotted lines indicate the maximum SLA in C^{CR} (from Fig. 5). The figure has been realized using the Ferret program (<http://ferret.pmel.noaa.gov/Ferret/>)

and disappeared in July 2021, with a maximum surface wind outflow ($> 1 \text{ m/s}$) in June 2021. On the western edge of the South Atlantic, counterbalancing northerly winds form the western side of a long-lasting anomalous low-pressure system (see Figs. 3 and 7e). Results from the forced sensitivity experiments already suggested that this atmospheric circulation is detrimental to the dynamics

of the 2021 coastal warming south of 16° S (Sect. 3.3). However, we now ask whether the atmospheric conditions south of 30° S may have had an impact on the equatorial variability leading up to the triggering of the 2021 Atlantic Niño event. To test this hypothesis, we conducted a sensitivity experiment, C^{SOUTH} (Table 2), in which the interannual variability of the WRF ABCs is restricted south of

CPL response assoc/wth ATM Southern fluxes

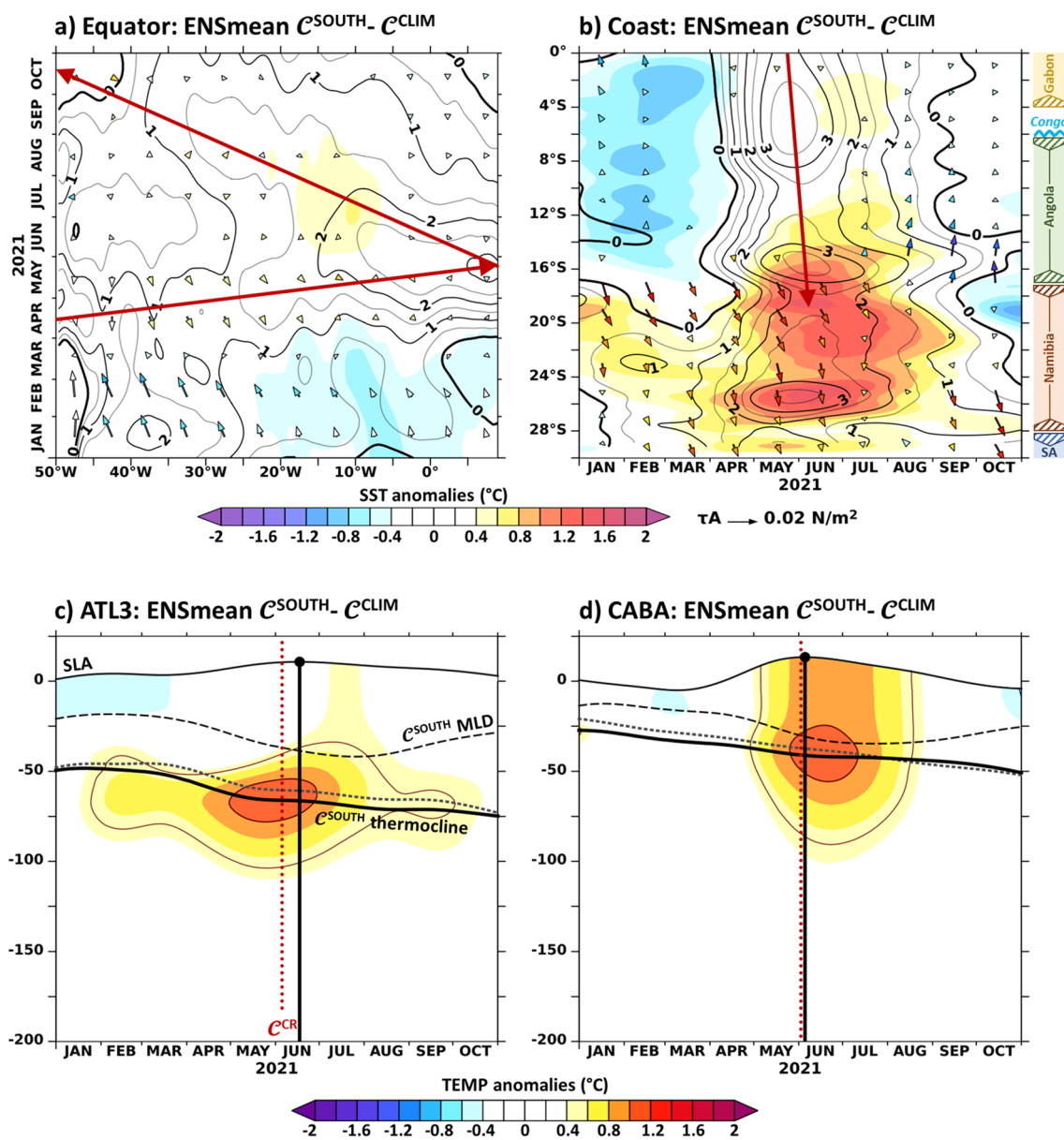


Fig. 9 Coupled response associated with southern atmospheric fluxes. Same as Fig. 8, but for the ensemble mean of the C^{SOUTH} simulations. In the upper panels, red dashed arrows show the equatorial (panel a) and coastal (panel b) wave propagations described in

Sect. 4.3. In the lower panels, the vertical red dotted lines indicate the maximum SLA in C^{CR} (from Fig. 5). The figure has been realized using the Ferret program (<http://ferret.pmel.noaa.gov/Ferret/>)

15° S (see the orange boundary lines Fig. 7c). Similar to C^{NW} , the [15° S–10° S] region serves as a linear transition zone between the southern region where the interannual variability is prescribed, and the northern region where the ABCs have been filtered. C^{SOUTH} interannual fluctuations shown in Fig. 9 can be compared to our coupled control simulation (C^{CR} , see Fig. 5). Results show that the 2021 interannual variability in C^{SOUTH} resembles that

of C^{CR} , both in the equatorial sector and along the West African coast, but with significantly reduced amplitude (Fig. 9ab). As indicated by the red arrows from C^{CR} , the timing of the equatorial and coastal C^{SOUTH} SLA propagations is in phase with the control run propagations. This confirms that the anomalous ABCs south of the tropical Atlantic (32° S) not only trigger the reduction in the SAA amplitude that, to a large extent, controlled the timing and

amplitude of the 2021 Benguela Niño, but also drive the relaxation of the equatorial trade at the origin of the 2021 Atlantic Niño.

A closer look at the differences between C^{SOUTH} (Fig. 9) and C^{CR} (Fig. 5) reveals that the 2021 Atlantic Niño variability of the sensitivity experiment is $\sim 50\text{--}80\%$ that of the control run. For instance, C^{SOUTH} (C^{CR}) maximum anomaly in ATL3 (Fig. 9c) is 2.2 cm (3.6 cm) for the SLA, 1.2 °C (1.9 °C) for the subsurface temperature, and 0.4 °C (0.5 °C) for the SST. In May 2021, the maximum C^{SOUTH} zonal wind stress anomaly in the WCEA ($+0.40 \times 10^{-2}$ N/m²) is slightly less than half that of C^{CR} ($+0.81 \times 10^{-2}$ N/m²). C^{SOUTH} equatorial variability is thus missing a source of interannual variability, which most likely ought to come from the suppressed interannual inflows at the northwestern boundary (Sect. 4.3). Along the equator, the zonal extent of the interannual changes in the Atlantic Walker cell actually extends westward beyond the position of our WRF western boundary, up to 80° W (Illig et al. 2006). In this context, the filtered C^{SOUTH} climatological conditions at the northwestern atmospheric boundary can be viewed as a wall in terms of interannual variability, preventing the full development of the air–sea interactions in the equatorial Atlantic and leading to a weakened EKW in April–May 2021 (Fig. 9a). As a consequence, the ocean coastal connection with the equatorial variability is also weakened in C^{SOUTH} compared to C^{CR} , which in turn explains the reduced interannual variability along the West African coast (Fig. 9b). In CABA (Fig. 9d), the averaged C^{SOUTH} (C^{CR}) maximum SLA, subsurface temperature, and SST anomalies are 2.8 cm, 1.1 °C, and 0.94 °C (5.0 cm, 1.8 °C, and 1.5 °C), respectively. Notably, the weaker coastal SSTA in C^{SOUTH} compared to C^{CR} leads to a shallower overlying MABL resulting in 15% stronger southward coastal wind stress within the [20° S–30° S] region in January–June 2021, minimizing the differences between C^{SOUTH} and C^{CR} .

The results of the C^{SOUTH} experiment revealed that the 2021 Atlantic Niño was triggered by the variability in the southern basin. However, the design of the C^{SOUTH} experiment does not allow to disentangle the effect of the atmospheric fluxes prescribed at the southern boundary (32° S) from that of the positive coastal SSTA associated with the Benguela Niño in shaping the equatorial variability in 2021. We now ask whether there is an atmospheric connection linking the Benguela Niño variability to the strength of the SAA and, in turn, to the Atlantic Niño variability, as proposed by Hu and Huang (2007). To quantify the impact of the coastal SSTA on the coupled equatorial dynamics, we created a sensitivity experiment, $C^{\text{SOUTH_noBN}}$ (Tab.2). $C^{\text{SOUTH_noBN}}$ shares the same ABCs as C^{SOUTH} , but in this experiment, WRF cannot see the interannual SST anomalies along the West African coast. Technically, the CROCO SST in the Southeast Atlantic ([5° W–20E; 30° S–9° S], see blue rectangle in Fig. 7c) is replaced by the hourly

SST of the C^{CLIM} ensemble mean when it is sent to WRF by the coupler. To smooth-out artificial SST gradients, a 4°-wide linear transition zone between the prescribed climatological SSTs and the actual $C^{\text{SOUTH_noBN}}$ SSTs simulated by CROCO is appended to the climatological SST domain. The difference between C^{SOUTH} (Fig. 9) and $C^{\text{SOUTH_noBN}}$ (Fig. 10) allows to quantify the effect of the southeastern SSTA on the equatorial variability. As expected, concealing the positive coastal SSTA from WRF yields to a lower overlying MABL, which locally weakens the coupling with the equatorward coastal tropospheric winds. Similar to Fig. 4d, the difference between C^{SOUTH} and in $C^{\text{SOUTH_noBN}}$ portrays equatorward coastal wind stress anomalies over the C^{SOUTH} positive SSTA (Fig. 10b). Interestingly, the southeastern coastal SSTA not only affects the local coastal atmospheric circulation, but also gives rise to a basin-wide weakening of the trade winds (Fig. 10d). In agreement with Hu and Huang (2007), the positive coastal SSTA triggers an anomalous low local SLP, which drives a converging lower-atmospheric circulation in the Southeast Ocean, producing westerly anomalies along the equator. As a result, the equatorial anomalies are much smaller in $C^{\text{SOUTH_noBN}}$ than in C^{SOUTH} (Fig. 10a). In May 2021, the $C^{\text{SOUTH_noBN}}$ maximum zonal wind stress anomaly is weaker in the WCEA ($+0.32 \times 10^{-2}$ N/m²) than in C^{SOUTH} ($+0.4 \times 10^{-2}$ N/m²). In ATL3, the maximum $C^{\text{SOUTH_noBN}}$ (C^{SOUTH}) anomaly is 1.6 cm (2.2 cm) for the SLA, 0.95 °C (1.2 °C) for the subsurface temperature, and 0.3 °C (0.4 °C) for the SST (Fig. 10ac).

In conclusion, our results reveal that the 2021 Atlantic and Benguela Niño events were both triggered by the atmospheric boundary fluxes at the southern boundary of our coupled domain ($\sim 32^\circ$ S). Local air–sea interactions yield a positive feedback in the equatorial band (Bjerknes feedback) and a negative feedback along the coast through the deepening of the coastal MABL. Furthermore, $\sim 1/3$ rd of the amplitude of the C^{SOUTH} equatorial variability can be attributed to the basin-wide atmospheric connection associated with the warm Benguela Niño coastal SSTA. The differences between C^{SOUTH} and C^{CR} showed that the amplitude of the 2021 Benguela Niño was in turn largely (40–50%) driven by the oceanic connection with the propagation of equatorially-forced CTW propagations, and thus also associated with the strength of the Atlantic Niño. Finally, the coastal variability is also shaped by the atmospheric teleconnection through the converging low-level atmospheric circulation associated with the equatorial warming.

5 Discussion and conclusions

In this paper, we analyzed the extreme Atlantic and Benguela Niño events that occurred during the boreal spring–summer of 2021. Based on observed detrended SSTA (OI-SST, Huang et al. 2021) in the

CPL response assoc/wth Southeastern Atlantic SSTA

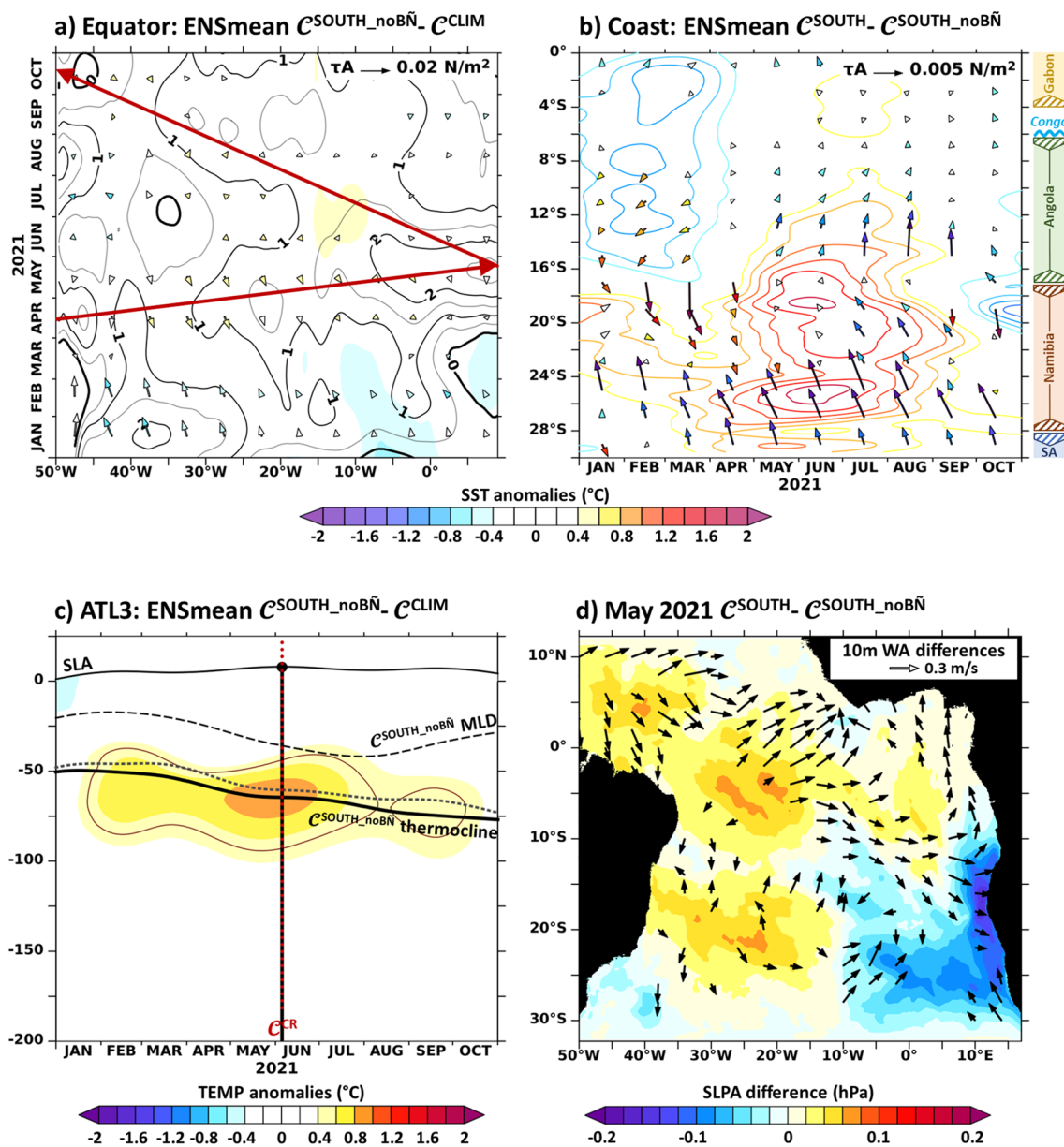


Fig. 10 Coupled response associated with southeastern Atlantic SSTA interannual anomalies. **a, c** Same as Fig. 8ac, but for the ensemble mean of the C^{SOUTH_noBN} simulations. **b** Same as Fig. 4d, but for the difference between C^{SOUTH} and C^{SOUTH_noBN} interannual anomalies. Colored contours correspond to C^{SOUTH} SSTA shown in Fig. 8b. **d**

May 2021 SLP (colors, hPa) and 10m wind (arrows, m/s) interannual anomaly difference between C^{SOUTH} and C^{SOUTH_noBN} . The figure has been realized using the Ferret program (<http://ferret.pmel.noaa.gov/Ferret/>)

eastern-equatorial Atlantic (ATL3) and along the Angolan/Namibian coasts (CABA), the 2021 Atlantic Niño set a new record as the warmest equatorial event since 1982, while the 2021 Benguela Niño ranked as the 6th warmest coastal event and was associated with the weakest boreal summer primary production since 2002 (Körner et al. 2023). Our objectives were to analyze the phenology of

these interannual events, the air–sea interactions at work, and the oceanic and atmospheric connections between the equatorial and the coastal warmings. To this end, we conducted no less than 10 complementary sensitivity experiments with a regional ocean–atmosphere coupled model. Forced and coupled ensemble simulations enabled us to identify the triggering mechanism of the 2021 events and

to quantify the roles played by both local and remote processes behind the equatorial and coastal warm events.

Our results revealed that the 2021 Atlantic and Benguela Niño events were both triggered by anomalous atmospheric fluxes at the southern boundary of our coupled model domain, at $\sim 32^\circ$ S, leading to a significant weakening of the SAA. The associated poleward anomalous low-level coastal winds began as early as February 2021, and led, through local processes (reduced upwelling and evaporation), to a warmer-than-normal coastal margin south of 16° S, off Angola, Namibia, and South Africa, marking the onset of the 2021 Benguela Niño. The weakening of the SAA was quite persistent, and it was not until April 2021 that the equatorial trade winds were affected. A relaxation of the WCEA zonal winds triggered the propagation of an initial downwelling EKW that crossed the equatorial basin in April–May 2021. Along its path, this wave deepened the thermocline and induced temperature anomalies in the eastern equatorial basin. This was the catalyst for the development of the 2021 Atlantic Niño. Classically, the full maturation of the equatorial event was driven by ENSO-like air–sea interactions in the equatorial basin: a positive feedback such that the warm eastern SSTA enhanced the westerly wind stress anomalies in the WCEA by modifying the Atlantic Walker cell (Bjerknes feedback). The warming in the eastern equatorial Atlantic peaked in mid-July 2021, with observed ATL3 SSTA exceeding 1.1°C . Furthermore, upon reaching the Gabonese coast, the EKW excited a downwelling CTW, which propagated southward along West Africa in May–June 2021 (Fig. 11a). This CTW warmed the northern coastal margin (north of 16° S) and further reinforced the locally-forced warm conditions already established in the southern coastal region. In the CABA region, the observed warming exceeded 1.4°C in late May 2021. Thus, the 2021 Benguela Niño was driven by the combined effects of surface wind anomalies and the propagation of the equatorially-forced CTW, which resulted in a banana-shaped pattern as described in Bachèlery et al. (2020). This sequence is consistent with the recent analyses by Li et al. (2023) of the 2019 and 2021 Atlantic Niño events.

Although our coupled simulations exhibited an excessively deep thermocline that prevented a realistic warming of the equatorial SST and most likely underestimated air–sea interaction associated with the Atlantic Niño warming, our study successfully unraveled the multiple factors that contributed to the remarkable strength of this particular warm event. Firstly, the long-term oceanic memory, associated with free-propagating downwelling equatorial waves forced prior to 2021, warmed the slightly colder-than-usual surface layer in the vicinity of the equatorial waveguide during the first trimester of 2021. This allowed neutral conditions to be reached in March 2021 – just before the onset of the equatorial event – facilitating the positive feedback

between positive SSTA in the Gulf of Guinea and trade wind relaxation in the WCEA (Fig. 11b). Additionally, while the colder than normal equatorial Pacific in 2021 may not have directly initiated the tropical Atlantic warming, it provided favorable conditions for the event to develop by facilitating the weakening of the Atlantic Walker cell thanks to anomalous inflows from the Pacific (Handoh and Bigg 2000; Illig et al. 2006). In fact, Li et al. (2023) quantified that 6% of the ATL3 anomalies during the period 2019–2021 can be explained by ENSO conditions. Concomitantly, the early development of the Benguela Niño south of 16° S induced a low coastal SLP, which drove low-level converging winds into the southeastern coastal ocean (see Fig. 11d; Hu and Huang 2007; Li et al. 2023). The resulting northwesterly inflow extended up to the equatorial band and contributed by $1/3^{\text{rd}}$ of the relaxation of the trade winds in April 2021. Finally, the timing of the triggering mechanism holds significant importance for the development of an Atlantic Niño. Indeed, the interannual equatorial ocean variability is phase-locked to the May–June–July season, characterized by a shallow thermocline and effective subsurface/surface coupling, enabling a strong Bjerknes feedback (Keenlyside and Latif 2007; Illig et al. 2020). In this context, the persistence of the intense anomalous coastal atmospheric outflow at 32° S, from February to June 2021, played a crucial role in the triggering of the equatorial event. Li et al. (2023) also emphasized the significant influence of interdecadal-trend components on the extreme magnitude 2021 Atlantic Niño event.

The coastal warming observed in 2021 was also one of the strongest Benguela Niño events observed since the satellite era. Our findings showed that its intensity can be attributed to two key mechanisms. Firstly, the external forcing at the southern boundary exhibited notable strength and persistence. It induced a substantial warming of the entire coastal margin from 16° S to the southern tip of Africa as early as February 2021. Secondly, because the amplitude of the coastal warming is directly related to the strength of the Atlantic Niño through the oceanic wave connection (Fig. 11a), the strong EKW associated with the strong Atlantic Niño gave way to a strong downwelling CTW, amplifying the event by approximately 40–50% in May–June 2021. It is worth noting that the local and remote air–sea interactions within the tropical Atlantic predominantly consist of negative feedback mechanisms for the maturation of the coastal warming. On one hand, the development of the anomalous converging circulation over the equatorial warming drives equatorward upwelling-favorable coastal winds north of 16° S (see Fig. 11c; Illig et al. 2020). On the other hand, the positive coastal SSTA also leads to intensified equatorward upwelling-favorable surface winds through the destabilization and deepening of the coastal MABL (Fig. 11e). However, it is important to acknowledge that both of these

Connection processes during the 2021 Atlantic and Benguela Niños

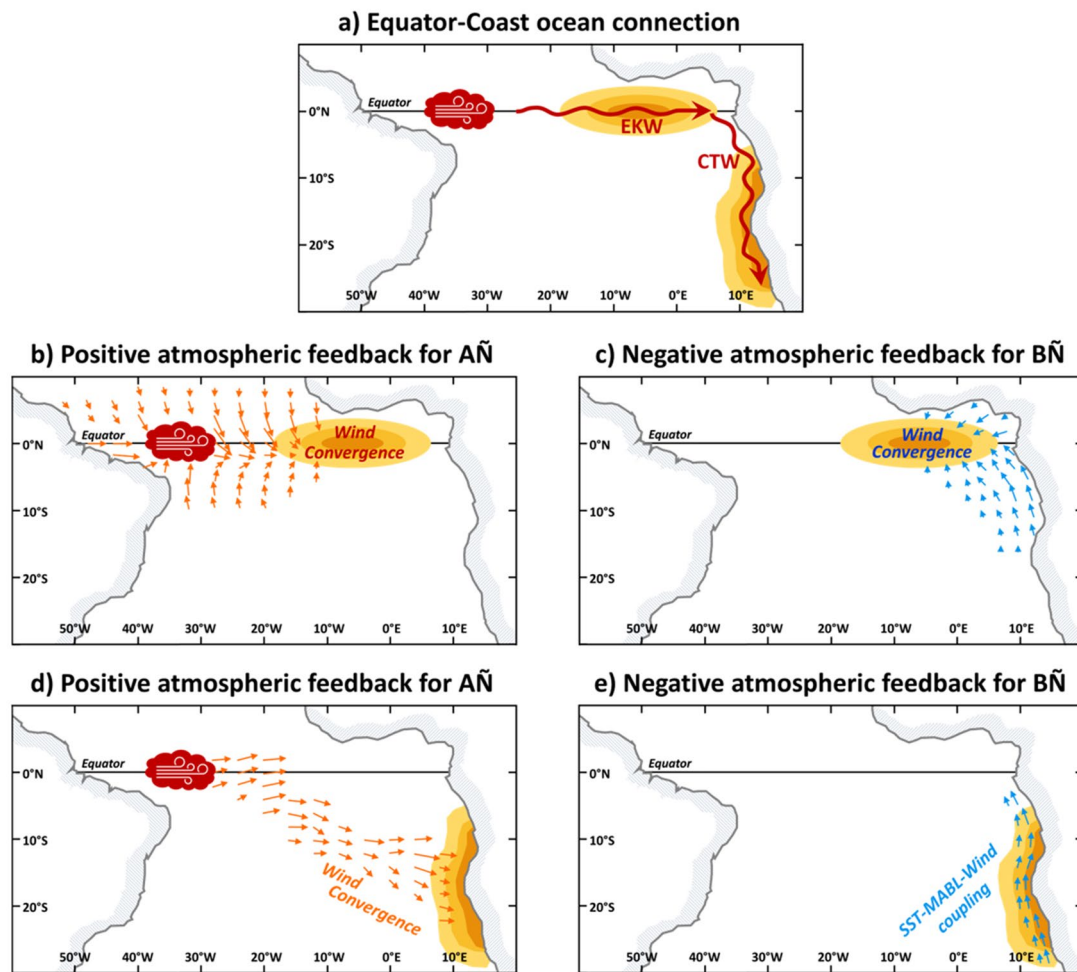


Fig. 11 Schematic of the 5 connection processes at work during the 2021 Atlantic and Benguela Niño events. **a** Oceanic connection between the equatorial dynamics and the coastal variability through long-wave propagations. **b** Positive atmospheric feedback associated with the equatorial warming: Development of an anomalous converging circulation towards the equatorial warming, whose western branch strengthens the trade wind relaxation in the WCEA. **c** Negative atmospheric feedback between Atlantic Niño and coastal warming: The southeastern branch of the anomalous equatorial con-

vergence drives equatorward upwelling-favorable coastal winds. **d**) Positive atmospheric feedback between the Benguela Niño SSTA and the equatorial wind forcing: The wind convergence towards the coastal warming weakens the trade winds up to the equatorial band. **e** Local negative atmospheric feedback associated with the coastal warming: Coupling between the high-altitude equatorward winds through the deepening of the coastal Marine Atmospheric Boundary Layer (MABL). The figure has been realized using Microsoft PowerPoint (<https://products.office.com/fr/powerpoint>)

processes may be underestimated in our coupled simulations due to the bias in the mean thermocline depth.

Overall, our case study highlights the intricate interplay between the ocean wave dynamics, and the local and distant air–sea interactions (Fig. 11), shedding light on the complex mechanisms that control the amplitude and timing of the Atlantic and Benguela Niño events. It also reveals the high degree of interconnectedness between the two distant systems. Indeed, we have shown that the Atlantic Niño dynamics affects the interannual coastal

variability, both through the equatorial/coastal oceanic wave connection (Fig. 11a) and through changes in the low-level coastal atmospheric circulation (Fig. 11c), as suggested by Illig et al. (2020). In turn, the SSTA associated with the Benguela Niño, although acting as a negative feedback for the coastal warming (Fig. 11e), positively influences the equatorial variability through the atmospheric teleconnection associated with the low coastal SLP and the associated low-level anomalous winds blowing towards the coastal warm event (Fig. 11d), as suggested

by Hu and Huang (2007). Adding the fact that the 2021 Atlantic and Benguela Niño events share the same external triggering mechanism, our results strongly suggest that these two interannual modes of variability are part of a unified mode of variability in the tropical Atlantic. However, both systems are based on different mean states that undergo distinct seasonal modulations, which also controls the surface expression of the variability. They are also vulnerable to different external forcings, which explains why Atlantic Niño events can occur independently of Benguela Niño events, and vice versa.

Our research contributes to a deeper understanding of the broader climate dynamics in the tropical Atlantic and to improving Earth system models, which currently struggle to simulate these extreme events. This knowledge can also ultimately enhance our ability to predict and manage the impacts of such extreme events on local ecosystems, fisheries, and socioeconomic activities along the affected coastlines. It underscores the importance of continued research in this field to support informed decision-making and safeguard the resilience of coastal communities in the face of climate change.

Supplementary Information The online version contains supplementary material available at <https://doi.org/10.1007/s00382-023-06934-0>.

Acknowledgements We would like to thank Lionel Renault (IRD/LEGOS) for his help in choosing the atmospheric model parameterizations and for fruitful discussions on coupled processes. This study has been carried out in the framework of the EU H2020 TRIATLAS project under grant agreement 817578. Marie-Lou Bachèlery has received funding from the European Union's Horizon 2020 Research and Innovation Program for the project BENGUP under the Marie Skłodowska-Curie grant agreement ID 101025655. Model computations were performed on CALMIP computer at University Paul Sabatier (Toulouse, France, CALMIP, project 19002). CROCO model grid, forcing, and initial conditions were built using the CROCO_Tools software (Penven et al. 2008). CROCO and CROCO_TOOLS can be downloaded from <https://www.croco-ocean.org>. Authors wish to acknowledge use of the Ferret program for analyses and graphics in this paper. Ferret is a product of NOAA's Pacific Marine Environmental Laboratory, available at <http://ferret.pmel.noaa.gov/Ferret>. AVISO Altimetric data, NOAA SST, CERSAT ASCAT wind stress, and WOA and CARS2009 climatologies are freely available to the public on the dedicated websites of these programs. resilience of coastal communities in the face of climate change.

Author contributions SI and M-LB conceived and designed the study. Material preparation, model simulations, and analyses were performed by SI. SI and M-LB co-wrote the paper.

Funding Open access funding provided by University of Cape Town. Marie-Lou Bachèlery has received funding from the European Union's Horizon 2020 Research and Innovation Program for the project BENGUP under the Marie Skłodowska-Curie grant agreement ID 101025655.

Data availability Due to their large size, the datasets generated and analyzed during the current study are not publicly available but are available from the corresponding author on reasonable request.

Declarations

Conflict of interest Serena Illig and Marie-Lou Bachèlery have no financial interests to disclose.

Open Access This article is licensed under a Creative Commons Attribution 4.0 International License, which permits use, sharing, adaptation, distribution and reproduction in any medium or format, as long as you give appropriate credit to the original author(s) and the source, provide a link to the Creative Commons licence, and indicate if changes were made. The images or other third party material in this article are included in the article's Creative Commons licence, unless indicated otherwise in a credit line to the material. If material is not included in the article's Creative Commons licence and your intended use is not permitted by statutory regulation or exceeds the permitted use, you will need to obtain permission directly from the copyright holder. To view a copy of this licence, visit <http://creativecommons.org/licenses/by/4.0/>.

References

- Bachèlery ML, Illig S, Dadou I (2016) Interannual variability in the South-East Atlantic Ocean, focusing on the Benguela Upwelling System: remote versus local forcing. *J Geophys Res Oceans* 121:284–310. <https://doi.org/10.1002/2015JC011168>
- Bachèlery ML, Illig S, Rouault M (2020) Interannual Coastal Trapped Waves in the Angola-Benguela Upwelling System and Benguela Niño and Niña events. *J Mar Syst* 203:103262. <https://doi.org/10.1016/j.jmarsys.2019.103262>
- Binet D, Gobert B, Maloueki L (2001) El Niño-like warm events in the Eastern Atlantic (6° N, 20° S) and fish availability from Congo to Angola (1964–1999). *Aquat Living Resour* 14:99–113
- Boyer DC, Boyer HJ, Fossen I, Kreiner A (2001) Changes in abundance of the northern Benguela sardine stock during the decade 1990–2000, with comments on the relative importance of fishing and the environment. *S Afr J Mar Sci* 23:76–84
- Brandt P, Caniaux G, Bourlès B, Lazar A, Dengler M, Funk A, Hormann V, Giordani H, Marin F (2011) Equatorial upper-ocean dynamics and their interaction with the West African monsoon. *Atmosph Sci Lett* 12:24–30. <https://doi.org/10.1002/asl.287>
- Burls NJ, Reason CJC, Penven P, Philander SG (2011) Similarities between the tropical Atlantic seasonal cycle and ENSO: an energetics perspective. *J Geophys Res* 116:C11010. <https://doi.org/10.1029/2011JC007164>
- Burmeister K, Lübbecke JF, Brandt P (2016) Revisiting the cause of the eastern equatorial Atlantic cold event in 2009. *J Geophys Res Ocean* 7:4777–4789. <https://doi.org/10.1002/2016JC011719>
- Carton J, Huang B (1994) Warm events in the tropical Atlantic. *J Phys Oceanogr* 24(5):888–903. [https://doi.org/10.1175/1520-0485\(1994\)024%3c0888:WEITTA%3e2.0.CO;2](https://doi.org/10.1175/1520-0485(1994)024%3c0888:WEITTA%3e2.0.CO;2)
- CERSAT (2002) Mean wind fields (MWF product) user manual volume 1: QuikSCAT.Rep C2-MUT-W-04-IF. CERSAT-IFREMER, Brest
- Chou M-D, Suarez MJ (1999) A solar radiation parameterization for atmospheric studies. NASA Tech. Memo.NASA/TM-1999-104606, Vol. 15, p 38. <http://gmao.gsfc.nasa.gov/pubs/docs/Chou136.pdf>. Accessed 08 June 2023
- Colberg F, Reason CJC, Rodgers K (2004) South Atlantic response to El Niño-Southern Oscillation induced climate variability in an ocean general circulation model. *J Geophys Res* 109:C12015. <https://doi.org/10.1029/2004JC002301>
- Craig A, Valcke S, Coquart L (2017) Development and performance of a new version of the OASIS coupler, OASIS3-MCT_3.0. *Geosci Model Dev* 10:3297–3308. <https://doi.org/10.5194/gmd-10-3297-2017>

- Debreu L, Marchesiello P, Penven P, Cambon G (2012) Two-way nesting in split-explicit ocean models: algorithms, implementation and validation. *Ocean Model* 49–50:1–21. <https://doi.org/10.1016/j.ocemod.2012.03.003>
- Dunn J (2009) CARS 2009: CSIRO Atlas of Regional Seas, <http://www.marine.csiro.au/~dunn/cars2009/>, Mar. Lab., Commonw. Sci. and Ind. Res. Organ., Hobart, Tasmania, Australia. Accessed 08 June 2023
- Dussin R, Barnier B, Brodeau L (2016) The making of Drakkar forcing set DFS5, DRAKKAR/MyOcean Rep. 01–04-16, Laboratoire de Glaciologie et Géophysique de l'Environnement, Grenoble, France
- Fairall CW, Bradley EF, Rogers DP, Edson JB, Young GS (1996) Bulk parameterization of air-sea fluxes for Tropical Ocean-Global Atmosphere Coupled-Ocean Atmosphere Response Experiment. *J Geophys Res* 101:3747–3764
- Florenchie P, Lutjeharms JRE, Reason CJC, Masson S, Rouault M (2003) The source of Benguela Niños in the South Atlantic Ocean. *Geophys Res Lett* 30:1505. <https://doi.org/10.1029/2003GL017172.10>
- Florenchie P, Reason CJC, Lutjeharms JRE, Rouault M (2004) Evolution of interannual warm and cold events in the southeast Atlantic Ocean. *J Clim* 17:2318–2334
- Foltz GR, McPhaden MJ (2010) Interaction between the Atlantic meridional and Niño modes. *Geophys Res Lett* 37:L18604. <https://doi.org/10.1029/2010GL044001>
- Gammelsrød T, Bartholomae CH, Boyer DC, Filipe VLL, O'Toole MJ (1995) Intrusion of warm surface water along the Angolan–Namibian coast in February–March 1995: the 1995 Benguela Niño, *South Afr. J Mar Sci* 19(1998):41–56
- Han J, Pan H-L (2011) Revision of convection and vertical diffusion schemes in the NCEP Global Forecast System. *Wea Forecasting* 26:520–533. <https://doi.org/10.1175/WAF-D-10-05038.1>
- Handoh IC, Bigg GR (2000) A self-sustaining climate mode in the tropical Atlantic, 1995–97: observations and modelling. *Q J R Meteorol Soc* 126:807–821
- Hersbach H, Bell B, Berrisford P et al (2020) The ERA5 global reanalysis. *Q J R Meteorol Soc* 146:1999–2049. <https://doi.org/10.1002/qj.3803>
- Hirst A, Hastenrath SL (1983) Atmosphere-Ocean mechanisms of climate anomalies in the Angola-Tropical Atlantic Sector. *J Phys Oceanogr* 13:1146–1157
- Hong S-Y, Lim J-OJ (2006) The WRF single-moment 6-class microphysics scheme (WSM6). *J Korean Meteor Soc* 42:129–151
- Hu Z-Z, Huang B (2007) Physical processes associated with the tropical Atlantic SST gradient during the anomalous evolution in the southeastern ocean. *J Clim* 20:3366–3378
- Huang B, Liu C, Banzon V, Freeman E, Graham G, Hankins B, Smith T, Zhang H-M (2021) Improvements of the daily optimum interpolation sea surface temperature (DOISST) version 21. *J Clim* 34(8):2923–2939. <https://doi.org/10.1175/JCLI-D-20-0166.1>
- Illig S, Bachèlery ML (2019) Propagation of subseasonal equatorially-forced coastal trapped waves down to the Benguela upwelling system. *Nat Sci Rep* 9:5306. <https://doi.org/10.1038/s41598-019-41847-1>
- Illig S, Dewitte B (2006) Local coupled equatorial variability versus remote ENSO forcing in an intermediate coupled model of the tropical Atlantic. *J Clim* 19:5227–5252. <https://doi.org/10.1175/JCLI3922.1>
- Illig S, Dewitte B, Ayoub N, du Penhoat Y, Reverdin G, Mey PD, Bonjean F, Lagerloef GSE (2004) Interannual long equatorial waves in the tropical Atlantic from a high-resolution ocean general circulation model experiment in 1981–2000. *J Geophys Res* 109:C02022. <https://doi.org/10.1029/2003JC001771>
- Illig S, Gushchina D, Dewitte B, Ayoub N, du Penhoat Y (2006) The 1996 equatorial Atlantic warm event: origin and mechanisms. *Geophys Res Lett* 33:L09701. <https://doi.org/10.1029/2005GL025632>
- Illig S, Bachèlery M-L, Lübbecke JF (2020) Why do Benguela Niños lead Atlantic Niños? *J Geophys Res Oceans* 125:e2019JC016003. <https://doi.org/10.1029/2019JC016003>
- Imbol Kougue RA, Illig S, Rouault M (2017) Role of interannual Kelvin wave propagations in the equatorial Atlantic on the Angola Benguela Current system. *J Geophys Res Oceans* 122:4685–4703. <https://doi.org/10.1002/2016JC012463>
- Imbol Kougue RA, Rouault M, Illig S, Rouault M, Brandt P, Jouanno J (2019) Benguela Niños and Benguela Niñas in forced ocean simulation from 1958 to 2015. *J Geophys Res* 124:5923–5951. <https://doi.org/10.1029/2019JC015013>
- Jousse A, Hall A, Sun F, Teixeira J (2016) Causes of WRF surface energy fluxes biases in a stratocumulus region. *Clim Dyn* 46:571–584. <https://doi.org/10.1007/s00382-015-2599-9>
- Junker T, Schmidt M, Mohrholz V (2015) The relation of wind stress curl and meridional transport in the Benguela upwelling system. *J Mar Syst* 143:1–6. <https://doi.org/10.1016/j.jmarsys.2014.10.006>
- Keenlyside N, Latif M (2007) Understanding equatorial Atlantic interannual variability. *J Clim* 20(1):131–142. <https://doi.org/10.1175/JCLI3992.1>
- Körner M, Brandt P et al (2023) Coastal trapped waves and tidal mixing control primary production in the tropical Angolan upwelling system, Submitted to *Sciences Advances* in July 2023
- Large WG, McWilliams JC, Doney SC (1994) Oceanic vertical mixing: a review and a model with a nonlocal boundary layer parameterization. *Rev Geophys* 32(4):363–403. <https://doi.org/10.1029/94RG01872>
- Li X, Hu Z-Z, Tseng Y-H, Liu Y, Liang P (2022) A historical perspective of the La Niña event in 2020/21. *J Geophys Res* 127(7):e2021JD035546. <https://doi.org/10.1029/2021JD035546>
- Li X, Tan W, Hu Z-Z, Johnson NC (2023) Evolution and prediction of two extremely strong Atlantic Niños in 2019–2021: impact of Benguela warming. *Geophys Res Lett* 50:e2023GL104215. <https://doi.org/10.1029/2023GL104215>
- Lim K-SS, Hong S-Y, Yoon J-H, Han J (2014) Simulation of the summer monsoon rainfall over East Asia using the NCEP GFS cumulus parameterization at different horizontal resolutions. *Wea Forecasting* 29:1143–1154. <https://doi.org/10.1175/WAF-D-13-00143.1>
- Lübbecke JF, Böning CW, Keenlyside NS, Xie S-P (2010) On the connection between Benguela and equatorial Atlantic Niños and the role of the South Atlantic Anticyclone. *J Geophys Res* 115:C09015. <https://doi.org/10.1029/2009JC005964>
- Lübbecke JF, Burls NJ, Reason CJC, McPhaden MJ (2014) Variability in the South Atlantic Anticyclone and the Atlantic Niño mode. *J Climate* 27(21):8135–8150. <https://doi.org/10.1175/JCLI-D-14-00202.1>
- Lübbecke JF, Rodríguez-Fonseca B, Richter I, Martín-Rey Marta M, Losada T, Polo I, Keenlyside NS (2018) Equatorial Atlantic variability—modes, mechanisms, and global teleconnections. *Wires Clim Change*. <https://doi.org/10.1002/wcc.527>
- Lübbecke JF, Brandt P, Dengler M, Kopte R, Lüdke J, Richter I, Sena Martins M, Tschipalanga PCM (2019) Causes and evolution of the southeastern tropical Atlantic warm event in early 2016. *Clim Dyn* 53:261–274. <https://doi.org/10.1007/s00382-018-4582-8>
- Lutz K, Jacobeit J, Rathmann J (2015) Atlantic warm and cold water events and impact on African west coast precipitation. *Int J Climatol* 35:128–141. <https://doi.org/10.1002/joc.3969>
- Martín-Rey M, Lazar A (2019) Is the boreal spring tropical Atlantic variability a precursor of the Equatorial Mode? *Clim Dyn* 53:2339–2353
- Martín-Rey M, Polo I, Rodríguez-Fonseca B, Losada T, Lazar A (2018) Is there evidence of changes in tropical Atlantic variability modes under AMO phases in the observational record? *J Clim* 31(2):515–536

- Mohino E, Rodríguez-Fonseca B, Losada T, Gervois S, Janicot S, Bader J, Chauvin F (2011) Changes in the interannual SST-forced signals on West African rainfall. *AGCM Intercomp Clim Dyn* 37:1707–1725
- Münnich M, Neelin JD (2005) Seasonal influence on the Atlantic ITCZ and equatorial South America. *Geophys Res Lett* 32:L21709. <https://doi.org/10.1029/2005GL023900>
- Nakanishi M, Niino H (2004) An improved Mellor-Yamada level-3 model with condensation physics: its design and verification. *Bound-Layer Meteorol* 112:1–31
- Nakanishi M, Niino H (2009) Development of an improved turbulence closure model for the atmospheric boundary layer. *J Meteorol Soc Japan* 87:895–912. <https://doi.org/10.2151/jmsj.87.895>
- Olson JB, Kenyon JS, Angevine WA, Brown JM, Pagowski M, Sušelj K (2019) A description of the MYNN-EDMF scheme and the coupling to other components in WRF-ARW. NOAA Tech. Memo. OAR GSD-61, p 42. <https://doi.org/10.25923/n9wm-be49>
- Penven P, Debreu L, Marchesiello P, McWilliams JC (2006) Evaluation and application of the ROMS 1-way embedding procedure to the Central California upwelling system. *Ocean Model* 12:157–187. <https://doi.org/10.1016/j.ocemod.2005.05.002>
- Penven P, Marchesiello P, Debreu L, Lefevre J (2008) Software tools for pre- and post-processing of oceanic regional simulations. *Environ Model Softw* 23:660–662
- Polo I, Rodríguez-Fonseca B, Losada T, Garcia-Serrano J (2008) Tropical Atlantic variability modes (1979–2002). Part I: time-evolving SST modes related to West African rainfall. *J Clim* 21(24):6457–6475. <https://doi.org/10.1175/2008JCLI2607.1>
- Richter I, Behera SK, Masumoto Y, Taguchi B, Komori N, Yamagata T (2010) On the triggering of Benguela Niños: remote equatorial versus local influences. *Geophys Res Lett* 37:L20604. <https://doi.org/10.1029/2010GL044461>
- Ridgway KR, Dunn JR, Wilkin JL (2002) Ocean interpolation by four-dimensional least squares—application to the waters around Australia. *J Atmos Oceanic Technol* 19(9):1357–1375
- Rouault M, Florenchie P, Fauchereau N, Reason CJC (2003) South East tropical Atlantic warm events and southern African rainfall. *Geophys Res Lett* 30:8009. <https://doi.org/10.1029/2002GL014840>
- Rouault M, Illig S, Bartholomae C, Reason CJC, Bentamy A (2007) Propagation and origin of warm anomalies in the Angola Benguela upwelling system in 2001. *J Mar Syst* 68(3–4):473–488. <https://doi.org/10.1016/j.jmarsys.2006.11.010>
- Rouault M, Servain J, Reason CJC, Bourlès B, Rouault MJ, Fauchereau N (2009) Extension of PIRATA in the tropical South-East Atlantic: an initial one-year experiment. *Afr J Mar Sci* 31(1):63–71. <https://doi.org/10.2989/AJMS.2009.31.1.5.776>
- Rouault M, Illig S, Lübbecke J, Imbol Koungue RA (2018) Origin, development and demise of the 2010–2011 Benguela Niño. *J Mar Syst* 188:39–48. <https://doi.org/10.1016/j.jmarsys.2017.07.007>
- Ruiz-Barradas A, Carton JA, Nigam S (2000) Structure of interannual-to-decadal climate variability in the tropical Atlantic sector. *J Clim* 13:3285–3297
- Servain J, Wainer I, Ayina HL, Roquet H (2000) The relationship between the simulated climate variability modes of the tropical Atlantic. *Int J Climatol* 20:939–953
- Shannon V, Nelson G (1996) The Benguela: large scale features and processes and system variability. In: Wefer G, Berger WH, Siedler G, Webb DJ (eds) *The South Atlantic: present and past circulation*. Springer, Berlin, p 644
- Shannon LV, Boyd AJ, Brundrit GB, Taunton-Clark J (1986) On the existence of an El Niño-type phenomenon in the Benguela system. *J Mar Res* 44:495–520
- Shchepetkin AF, McWilliams JC (1998) Quasi-monotone advection schemes based on explicit locally adaptive dissipation. *Mon Weather Rev* 126:1541–1580
- Shchepetkin AF, McWilliams JC (2005) The regional oceanic modeling system (ROMS): a split-explicit, free-surface, topography-following-coordinate oceanic model. *Ocean Model* 9:347–404. <https://doi.org/10.1016/j.ocemod.2004.08.002>
- Skamarock WC, Klemp JB, Dudhia J, Gill DO, Barker D, Duda MG, Powers JG (2008) A Description of the Advanced Research WRF Version 3 (No. NCAR/TN-475+STR). University Corporation for Atmospheric Research. <https://doi.org/10.5065/D68S4MVH>
- Song Q, Aiki H (2023) Equatorial wave diagnosis for the Atlantic Niño in 2019 with an ocean reanalysis. In: Submitted to *Ocean Science*. 10.5194/egusphere-2023-1061
- Song Q, Aiki H, Tang Y (2023) The role of equatorially forced waves in triggering Benguela Niño/Niña as investigated by an energy flux diagnosis. *J Geophys Res Oceans* 128:e2022JC19272. <https://doi.org/10.1029/2022JC019272>
- World Meteorological Organization (2022) *State of the Climate in Africa 2021*, WMO-No 1300. Switzerland, 2022, ISBN 978-92-63-11300-9
- Zebiak SE (1993) Air–sea interaction in the equatorial Atlantic region. *J Clim* 6:1567–1586. [https://doi.org/10.1175/1520-0442\(1993\)006%3c1567:AIITEA%3e2.0.CO;2](https://doi.org/10.1175/1520-0442(1993)006%3c1567:AIITEA%3e2.0.CO;2)

Publisher's Note Springer Nature remains neutral with regard to jurisdictional claims in published maps and institutional affiliations.

Supporting Information for

“ The 2021 Atlantic Niño and Benguela Niño Events: External forcings and air-sea interactions “

Serena Illig^{1,2} and Marie-Lou Bachèlery³

¹ Laboratoire d’Etudes en Géophysique et Océanographie Spatiale (LEGOS),
CNRS/IRD/UPS/CNES, Toulouse, France. serena.illig@ird.fr

² Department of Oceanography, MARE Institute, LMI ICEMASA,
University of Cape Town, Rondebosch, South Africa.

³ Geophysical Institute, University of Bergen and Bjerknes Centre for Climate Research,
Bergen, Norway

Submitted to *Climate Dynamics* in June 2023

Manuscript revised in July 2023

Introduction

These **supplementary materials** provide a validation exercise that illustrates the realism of the tropical Atlantic Ocean and Atmosphere model configurations used in the study, specifically from an oceanographic perspective.

In **Supplementary Material S2**, we compare the mean state of our forced and coupled ocean-atmosphere simulations with the observations presented in **Supplementary Material S1**. **Supplementary Material S3** is devoted to the evaluation of the realism of the interannual variability. We focus our analysis on the key parameters related to the ocean-atmosphere dynamics that are relevant to our study, i.e. the ocean stratification, the surface heat and momentum surface fluxes, the sea level, and SST interannual variability.

As a reminder, our CROCO ocean configuration at $1/12^\circ$ is the same as that used in Illig et al. (2020), except that it is based on version 1.2 of the CROCO code. In the forced simulations, we use surface fluxes from COARE 3.0 bulk formulae (Fairall et al. 1996) based on 3-hour ERA5 fields (Hersbach et al. 2020), corrected in the manner of DRAKKAR Forcing Set v5 (Dussin et al. 2016; hereafter ERA5c). Our $1/4^\circ$ -resolution WRF atmospheric configuration includes the ocean domain and is constrained at its boundaries by 3-hour ERA5 fields.

As recalled in **Table S1**, we conducted two families of forced and coupled experiments: 1) interannual simulations where the forcing at the ocean surface and at the atmospheric lateral boundaries is interannual; and 2) climatological simulations in which CROCO is forced by climatological fields and the interannual variations at the WRF open boundaries have been filtered out. The latter one provides the seasonal mean state from which the 2021 interannual anomalies stray. First, long forced ocean simulations are run over the period 2012-2021. By

perturbing their respective temperature fields on January 1, 2020, CROCO^{INTER} and CROCO^{CLIM} spawn 5 ensemble forced simulations. Over the year 2021, their Sea Surface Temperatures (SST) serve as boundary conditions for WRF, so that the ensemble means of $\mathcal{F}^{\text{INTER}}$ and $\mathcal{F}^{\text{CLIM}}$ forced ocean-atmosphere experiments are used to study the ocean dynamics and atmospheric response during the 2021 Atlantic and Benguela Niño events. To investigate the respective roles of air-sea interactions and external forcing, \mathcal{C}^{CR} and $\mathcal{C}^{\text{CLIM}}$ coupled simulations are also performed for the year 2021.

NAME	Design	Period	Restart	CROCO surface forcing	WRF ABCs	Ens. Sim.
CROCO ^{INTER}	CROCO only	2012-2021	CARS2009	Interannual	N/A	1
↳ Spawn CROCO ^{INTER-2020}		2020	CROCO ^{INTER}	Interannual	N/A	5
$\mathcal{F}^{\text{INTER}}$	CROCO $\xrightarrow{\text{SST}}$ WRF	2021	CROCO ^{INTER-2020}	Interannual	Interannual	5
\mathcal{C}^{CR}	CROCO \Leftrightarrow WRF	2021	CROCO ^{INTER-2020}	From WRF	Interannual	5
CROCO ^{CLIM}	CROCO only	2012-2021	CARS2009	Climatological	N/A	1
↳ Spawn CROCO ^{CLIM-2020}		2020	CROCO ^{CLIM}	Climatological	N/A	5
$\mathcal{F}^{\text{CLIM}}$	CROCO $\xrightarrow{\text{SST}}$ WRF	2021	CROCO ^{CLIM-2020}	Climatological	No interannual	5
$\mathcal{C}^{\text{CLIM}}$	CROCO \Leftrightarrow WRF	2021	CROCO ^{CLIM-2020}	From WRF	No Interannual	5

Table S1: Subset of Table 1. Set of forced model experiments: Name of the experiment, design of the experiment (forced or coupled), period of the simulations, origin of CROCO restart, CROCO surface forcing (include or not interannual frequencies), WRF Atmospheric Boundary Conditions (ABCs, include or not interannual frequencies), and number of ensemble simulations.

S1: Data used to perform a validation exercise

A set of data is used to assess the ability of our ocean model configuration to represent the observed most salient features of the tropical Atlantic Ocean, relevant to the purpose of our study.

To evaluate the realism of the mean state of our most realistic forced simulation CROCO^{INTER}, we compare the outputs with the World Ocean Atlas 2023 (WOA, Locarnini et al. 2023). WOA is a long-term set of objectively analyzed climatological fields built from observed oceanographic profile data interpolated to standard depths on regular horizontal grids. We downloaded the mean temperature for the period 1991-2020 on a 0.25° grid from the NOAA National Centers for Environmental Information (<https://www.ncei.noaa.gov/access/world-ocean-atlas-2023>).

The model interannual SST is compared to the daily global analysis product blended with AVHRR data, OISST version 2 (also known as Reynolds_AVHRR'SST, Huang et al. 2021) over the period 2012-2021. This product merges SST observations from remote-sensed

AVHRR observations and *in situ* platforms (ships and buoys). The latter are interpolated onto a 0.25° grid and extrapolated using Optimal Interpolation at the NOAA National Centers for Environmental Information. The data were downloaded from the <http://apdrc.soest.hawaii.edu> data server.

We use the AVISO daily altimeter satellite gridded product to evaluate of the model Sea Level Anomaly (SLA) over the period 2012-2021. The AVISO SLA is estimated by optimal interpolation by merging the L3 along-track measurement from the different altimeter missions available on a $1/4^\circ \times 1/4^\circ$ Mercator grid (Pujol et al. 2016). This product is processed by the DUACS multimission altimeter data processing system and distributed by the Copernicus marine data store (<https://data.marine.copernicus.eu>).

ASCAT gridded data are compared with model surface momentum fluxes. ASCAT daily wind and wind stress fields are estimated over the global oceans since 2009 from Metop/ASCAT retrievals using an objective method (Bentamy and Croize-Fillon 2012). The calculation of daily estimates uses both ascending and descending available and valid retrievals. The resulting fields have a spatial resolution of 0.25° in longitude and latitude. The data are freely available from the Cersat/Ifremer ftp (<ftp://ftp.ifremer.fr/ifremer/cersat/products/gridded/MWF/L3/ASCAT/Daily>).

S2: Evaluation of $\mathcal{F}^{\text{CLIM}}$ and $\mathcal{C}^{\text{CLIM}}$ mean states

In this section, we evaluate the performances of our tropical Atlantic CROCO and WRF configurations in representing the mean ocean and atmospheric states in the equatorial Atlantic and along the southwest coast of Africa. We focus our analyses on the ocean stratification, which controls the ocean wave dynamics, and the flux exchanges at the ocean-atmosphere interface, i.e. the mean SST and the mean momentum and heat fluxes. We first evaluate the ensemble mean from $\mathcal{F}^{\text{CLIM}}$, which provides the mean state from which anomalies are estimated in the forced context. We then analyze the expected deviation of the ocean mean state in the coupled context ($\mathcal{C}^{\text{CLIM}}$). It is worth noting that the mean ocean state simulated by $\mathcal{F}^{\text{CLIM}}$ is very close to the CROCO^{INTER} mean state estimated for the period 2012-2021 (not shown).

The realism of $\mathcal{F}^{\text{CLIM}}$ mean SST is assessed against WOA mean SST. The model realistically represents the mean heat distribution in the tropical Atlantic (**Fig.S1a**), characterized by warm waters over the equatorial band that progressively cool towards the pole. The Benguela Upwelling System (BUS) is well represented along the coasts of Angola and Namibia ($[18^\circ\text{S}-30^\circ\text{S}]$) with cold surface waters. Maximum differences between modeled and observed SST remain below 1°C (**Fig.S1b**), except in the western equatorial basin and in the northern BUS coastal fringe, where the model is $\sim 1.5^\circ\text{C}$ colder and warmer than the observations, respectively. Along the coast of the northern Gulf of Guinea, the bias exceeds 2°C . We then evaluate the model mean vertical stratification along the equatorial and coastal waveguides which controls the characteristics of the equatorial and coastal waves (modal contribution, phase speed, modal scattering...). We compare $\mathcal{F}^{\text{CLIM}}$ mean vertical temperature sections with the WOA observations in the upper 250 m (**Fig.S1cd**). The results show a good representation of the mean vertical temperature structure in the equatorial band ($[3^\circ\text{S}-3^\circ\text{N}]$). The thermocline (position of the maximum vertical thermal gradients, blue lines in **Fig.S1d**) is well positioned along the equatorial waveguide. In agreement with the observations, the

modeled thermocline is deeper in the western equatorial Atlantic and shallower in the Gulf of Guinea with warm waters in the upper layers and cold waters below (**Fig.S1c**). On average over [45°W-8°E], $\mathcal{F}^{\text{CLIM}}$ 20°C-isotherm is 1.5 m deeper than the observations. The maximum differences between model and observations are localized in the vicinity of the thermocline (**Fig.S1d**) and remain less than 1.5°C. This bias is attributed to a typical weaker vertical stratification associated with a too diffuse thermocline: over [45°W-8°E], the layer comprised between the 16°C and 24°C isotherms is 13% thicker than in WOA. In the 2°-wide coastal margin off Angola between 10°S and 15°S, the mean temperature bias exceeds 1.5°C, symptomatic of a modeled vertical thermal structure that is too smooth compared to the observations. This bias may be attributed to the relatively weak spatial resolution of our configuration (1/12°) compared to the horizontal scales of the frictional boundary layer along the slope (~5km, Marchesiello and Estrade 2010).

WRF response to $\mathcal{F}^{\text{CLIM}}$ SST and to filtered ERA5 open conditions is now evaluated against the actual CROCO forcing derived from ERA5 (hereafter referred to as CROCO^{ERA5c}). WRF mean surface wind stress (**Fig.S2a**) is in good agreement with ERA5c, especially in terms of wind stress direction. The amplitude is also in good agreement with ERA5c, particularly in the equatorial region and along West Africa. The maximum differences are associated with weaker surface winds, localized in the western part of the domain, in the lower branches of the anticyclones on both sides of the equator (**Fig.S2c**). WRF and ERA5c mean solar (contours) and net surface heat fluxes (colors) at the sea surface are shown in the lower panels of **Fig.S2**. The mean heat distribution is well represented in WRF compared to ERA5c, with maximum heat uptake by the ocean in the equatorial band and along the African coast. However, the solar heat flux is strongly underestimated by an average of 45 W/m² over most of the domain. As a result, the net surface heat flux at the ocean boundary is significantly lower in WRF than in ERA5c, with an average bias of -50 W/m².

In the coupled context, starting from January 1, 2021, we expect an adjustment of the mean state of the ocean associated with an equilibration of the heat and momentum fluxes between the ocean and atmosphere components. Due to the biases in the WRF surface heat fluxes, the mean state in $\mathcal{C}^{\text{CLIM}}$ is substantially colder than in $\mathcal{F}^{\text{CLIM}}$ (by 1.4°C on average over the CROCO domain). The first 250-meter monthly temperature from $\mathcal{F}^{\text{CLIM}}$ and $\mathcal{C}^{\text{CLIM}}$ in the eastern equatorial sector (ATL3 box, [20°W-0°E; 3°S-3°N], **Fig.S3a**) and along the Angolan coast (CABA box, [10°S-20°S, 2° wide coastal margin, **Fig.S3c**]) show that the $\mathcal{C}^{\text{CLIM}}$ seasonal cycle remains very well in phase with $\mathcal{F}^{\text{CLIM}}$ (and with the observations, see Supplementary Material in Illig et al. 2020, their Figure S2), with warmer (colder) conditions in February-April (July-August), and maximum vertical thermal gradients from February to May. Notably, in both regions, $\mathcal{C}^{\text{CLIM}}$ has a deeper thermal structure with weaker thermal gradients than $\mathcal{F}^{\text{CLIM}}$, a classic bias of coupled models. The differences in the first 250-meter temperature between $\mathcal{C}^{\text{CLIM}}$ and $\mathcal{F}^{\text{CLIM}}$ (**Fig.S3bd**) do not show a large trend $\mathcal{C}^{\text{CLIM}}$ over 2021. On the contrary, a seasonal pattern of colder surface waters and a warmer thermocline in the boreal spring and fall emerges, accentuating the seasonal vertical gradient bias. Notably, it takes less than 3 months for CROCO to adjust to the WRF air-sea fluxes, before the onset of the 2021 Atlantic and Benguela Niños.

S3: Evaluation of $\text{CROCO}^{\text{INTER}}$, $\mathcal{F}^{\text{INTER}}$, and \mathcal{C}^{CR} interannual variability

The realism of the interannual variability along the equatorial and coastal wave propagation path is examined in **Fig.S4**. For a complete description of the methodology used to calculate the interannual anomalies, please refer to **Section 2.5** of the manuscript. Note that we have removed the linear trends from the interannual time series to avoid biases in the correlation estimation. **Fig.S4a** illustrates the good coherence between $\text{CROCO}^{\text{INTER}}$ interannual SLA and altimetric observations from 2012 to 2021 in the eastern-equatorial sector (ATL3 box) and along the Angolan coast (CABA box). The model represents the sequence of warm and cold events very well, with a highly significant correlation of 0.83 and 0.75 in ATL3 and CABA, respectively. In particular, the SLA increase associated with the 2021 equatorial event is captured by the 5 $\mathcal{F}^{\text{INTER}}$ ensemble members. In agreement with the altimetric data, the $\mathcal{F}^{\text{INTER}}$ ensemble mean peaks in June 2021 in ATL3 and in May 2021 in CABA, with the model leading the observations by less than a week. In the eastern equatorial Atlantic, the amplitude of the model interannual SLA variability is underestimated by $\text{CROCO}^{\text{INTER}}$, with a model/observation standard deviation ratio of 0.75 over the period 2012-2021 (cf. open maroon square in **Fig.S4b**). Notably, the $\text{CROCO}^{\text{INTER}}$ SLA increase in 2021 does not exceed +2.2cm, while it reaches +3.8 cm in the observations. In contrast, the model interannual variability in CABA is slightly larger (15%) than in the observations (cf. open blue circle in **Fig.S4b**), and the 2021 warm event is associated with SLA anomalies of +2cm (+1.76cm) in $\text{CROCO}^{\text{INTER}}$ (AVISO).

Fig.S4b further presents the model/observation comparison for the interannual SLA time series at each longitude in the eastern-equatorial sector from 20°W to 8°E (squares) and at each latitude along the coast of southwestern Africa from 0°N to 30°S (circles) using a Taylor diagram (Taylor 2001). Along the equator, the results show a good agreement between model and altimetric data with Taylor scores above 0.8 (see Eq.4 of Taylor 2001). Correlations remain largely above the 99% confidence level (Sciremammano 1979), but the magnitude of the interannual variability is underestimated by the model. Along the coast of southwestern Africa, interannual SLAs are also in very good agreement with the observations with Taylor scores above 0.7. The marginally lower agreement in the Benguela upwelling system is most likely due to the strong local mesoscale activity whose features, in the absence of data assimilation, cannot agree in space and time with AVISO data.

The ability of $\text{CROCO}^{\text{INTER}}$ to simulate the observed interannual SST fluctuations is assessed in **Fig.S4d** for the ATL3 and CABA domains over the period 2012-2021. The results show that the model agrees remarkably well with the observations, both in terms of amplitude and coherence, with Taylor scores greater than 0.9 in both regions (cf. open maroon square and open blue circle in **Fig.S4c**). The 2021 Atlantic and Benguela Niño events are well simulated by the model. While the phase and the amplitude of the coastal event are in very good agreement with the observations, the amplitude of the equatorial event is underestimated by the model and its peak occurs 3 weeks before the observations. The Taylor diagram shown in **Fig.S4c** confirms the realism of the interannual SST variations along the equatorial and coastal waveguides, with Taylor scores greater than 0.8.

The wind stress forcing from $\text{CROCO}^{\text{INTER}}$ and $\mathcal{F}^{\text{INTER}}$ ($\text{CROCO}^{\text{ERA5c}}$) is compared with the ASCAT data in **Fig.S4e**. Both in the western-central equatorial Atlantic and along the Angolan coast, the interannual momentum forcing is in very good agreement with the

observations, with statistically significant correlations above 0.9. However, we note that CROCO^{ERA5c} slightly overestimates the wind stress interannual variability, with standard deviation ratios of 117% and 108% in ATL3 and CABA regions, respectively. Of particular interest is the $\mathcal{F}^{\text{INTER}}$ WRF response to CROCO $\mathcal{F}^{\text{INTER}}$ SST and ERA5 open conditions that is shown in 2021 for the 5 ensemble simulations (thin gray lines). The interannual anomalies, computed relative to $\mathcal{F}^{\text{CLIM}}$, are in good agreement with the CROCO^{ERA5c} and ASCAT, capturing the relaxation of the WCEA trade winds from April to October 2021, with two maxima in May-June and in September-October, respectively. Whilst the $\mathcal{F}^{\text{INTER}}$ SSTA in the eastern equatorial Atlantic is lower than the observed anomalies (**Fig.S4d**), the amplitude of the WCEA zonal wind stress anomalies in July is larger in the WRF response, compared to the observations. Along the Angolan coast, WRF reproduces the southward anomalous circulation during the first semester of 2021, followed by a meridional wind stress reversal with upwelling favorable winds in the second half of the year. The amplitude of the coastal wind stress anomalies is in good agreement with the observations, but the wind reversal occurs ~1 month later than in CROCO^{ERA5c} and ASCAT.

Our focus now is on the interannual anomalies that occurred in the tropical Atlantic during the boreal spring and summer of 2021. **Fig.S5** shows the 2021 Atlantic Niño and Benguela Niño events as observed (**Fig.S5ab**) and as simulated by our forced ($\mathcal{F}^{\text{INTER}}$, **Fig.S5cd**) and coupled (\mathcal{C}^{CR} , **Fig.S5ef**) simulations. The aim here is not to describe the dynamics of these events, but only to comment on the agreement between model and observations along the equatorial and coastal waveguides.

In the equatorial belt (**Fig.S5a**), the observed signal shows a sequence of interannual anomalies consistent with the propagation of wind-driven equatorial downwelling waves propagation that imprint the SST. Positive SST anomalies develop in the Gulf of Guinea starting in May 2021. By mid-July, they exceed 1.3°C at 10°W. This warming is accompanied by a sea level rise of more than 4cm in the altimetric signal, peaking in June 2021. These ocean anomalies are associated with positive surface wind stress anomalies confined to the western-central basin. The relaxation of the trade winds begins in June 2021 and persist after October 2021. The forced model (**Fig.S5b**) realistically reproduces the main features of the equatorial dynamics, with timing and amplitude in good agreement with the observations. However, we note that the SLA peak slightly before the observed signal and that the eastern boundary SLA peaks in the second half of May, while it occurs one month later in the AVISO data. The warming also starts earlier in $\mathcal{F}^{\text{INTER}}$ compared to the OISST data and it also has a smaller zonal extent. The WRF response reproduces the relaxation of the western trade wind well, but the wind stress fluctuations start ~1 month earlier in WRF than in CROCO^{ERA5c}. In a coupled context (**Fig.S5c**), with a deeper thermocline (see **Section S2**), there is less communication between the wave-induced sub-surface anomalies and the surface mixed layer. As a result, the 2021 Atlantic Niño in \mathcal{C}^{CR} has a weaker amplitude than in the observations or in $\mathcal{F}^{\text{INTER}}$, with a maximum amplitude of 0.85°C at 10°W in late June. The wind-stress anomalies are also underestimated, most likely due to the reduced Bjerknes feedback. Despite this amplitude bias, the coupled model is able to simulate the 2021 Atlantic Niño with a timing in relatively good agreement with the observations. In particular, the \mathcal{C}^{CR} -SLA anomalies nicely show the

downwelling Kelvin wave propagation in April-May 2021, followed by a westward-propagating Rossby wave that imprints the SST.

Along the Angolan coast, the observations show that the 2021 Benguela Niño is characterized by a warming exceeding 1.5°C that starts south of 15°S in March-April 2021, associated with intense southward coastal wind-stress anomalies (**Fig.S5b**). The latter are associated with positive SLA, typical of downwelling conditions. In the north, the increase in the sea level and the warming begins one month later, resulting in a banana-shaped pattern of SSTA and SLA, as described in Bachèlery et al. (2020). Notably, the meridional wind stress anomalies are substantially smaller in the north than in the south, and an upwelling-favorable equatorward flow is observed, most likely associated with the equatorial warming (Illig et al. 2020). As previously reported, WRF realistically simulates the southward wind stress anomalies in $\mathcal{F}^{\text{INTER}}$ (**Fig.S5d**) and \mathcal{C}^{CR} (**Fig.S5f**), but their amplitude is overestimated compared to the observations and they start one month earlier. In $\mathcal{F}^{\text{INTER}}$, the equatorward winds are overestimated, which is not the case in the coupled simulation. In addition, the concave SSTA and SLA patterns are less pronounced in the simulations, and especially the warming in the northern coastal region is underestimated in the \mathcal{C}^{CR} . Nonetheless, the general features of the 2021 Benguela Niño are well captured by both the forced and coupled simulations, with magnitude and timing consistent with the observations.

In conclusion, the overall good agreement between our key simulations and the observations implies that the equatorial and coastal ocean dynamics are adequately simulated by our model configuration. This gives confidence to perform sensitivity experiments in order to assess the ocean-atmosphere connection during the 2021 Atlantic Niño and Benguela Niño events.

References:

- Bachèlery, ML., S. Illig and M. Rouault, 2020: Interannual Coastal Trapped Waves in the Angola-Benguela Upwelling System and Benguela Niño and Niña events. *Journal of Marine Systems*, Vol 203, March 2020, 103262, <https://doi.org/10.1016/j.jmarsys.2019.103262>.
- Bentamy, A., and D. Croze-Fillon, 2012: Gridded surface wind fields from Metop/ASCAT measurements. *Int. J. Remote Sens.*, 33, 1729–1754.
- Fairall, C. W., E. F. Bradley, D. P. Rogers, J. B. Edson and G. S. Young, 1996, Bulk parameterization of air-sea fluxes for Tropical Ocean-Global Atmosphere Coupled-Ocean Atmosphere Response Experiment. *J. Geophys. Res.*, 101, 3747–3764.
- Hersbach, H, Bell, B, Berrisford, P, et al. The ERA5 global reanalysis. *Q J R Meteorol Soc.* 2020; 146: 1999– 2049. <https://doi.org/10.1002/qj.3803>.
- Huang, B., C. Liu, V. Banzon, E. Freeman, G. Graham, B. Hankins, T. Smith, and H.-M. Zhang, 2021: Improvements of the Daily Optimum Interpolation Sea Surface Temperature (DOISST) Version 2.1. *J. Climate*, 34(8), 2923-2939. DOI: 10.1175/JCLI-D-20-0166.1.

- Illig, S., M.-L. Bachèlery and J. F. Lübbecke, 2020: Why do Benguela Niños lead Atlantic Niños? *Journal of Geophysical Research: Oceans*, 125, e2019JC016003. <https://doi.org/10.1029/2019JC016003>.
- Locarnini, R. A., O. K. Baranova, A. V. Mishonov, T. P. Boyer, J. R. Reagan, D. Dukhovskoy, D. Seidov, H. E. Garcia, C. Bouchard, S. Cross, C. R. Paver, and Z. Wang, 2023. *World Ocean Atlas 2023, Volume 1: Temperature*. A. Mishonov Technical Ed. NOAA Atlas NESDIS (in preparation).
- Marchesiello, P., and P. Estrade (2010), Upwelling limitation by geostrophic onshore flow, *J. Mar. Res.*, 68, 37–62.
- Pujol, M.-I. et al. DUACS DT2014: the new multi-mission altimeter data set reprocessed over 20 years. *Ocean Sci.*12, 1067–1090 (2016).
- Sciremammano, F. A Suggestion for the Presentation of Correlations and Their Significance Levels. *J. Phys. Oceanogr.* 9, 1273-1276 (1979).
- Taylor, K. E. Summarizing multiple aspects of model performance in a single diagram. *J. Geophys. Res.* 106, 7183–7192 (2001).

Figures

Validation of CROCO mean state from $\mathcal{F}^{\text{CLIM}}$

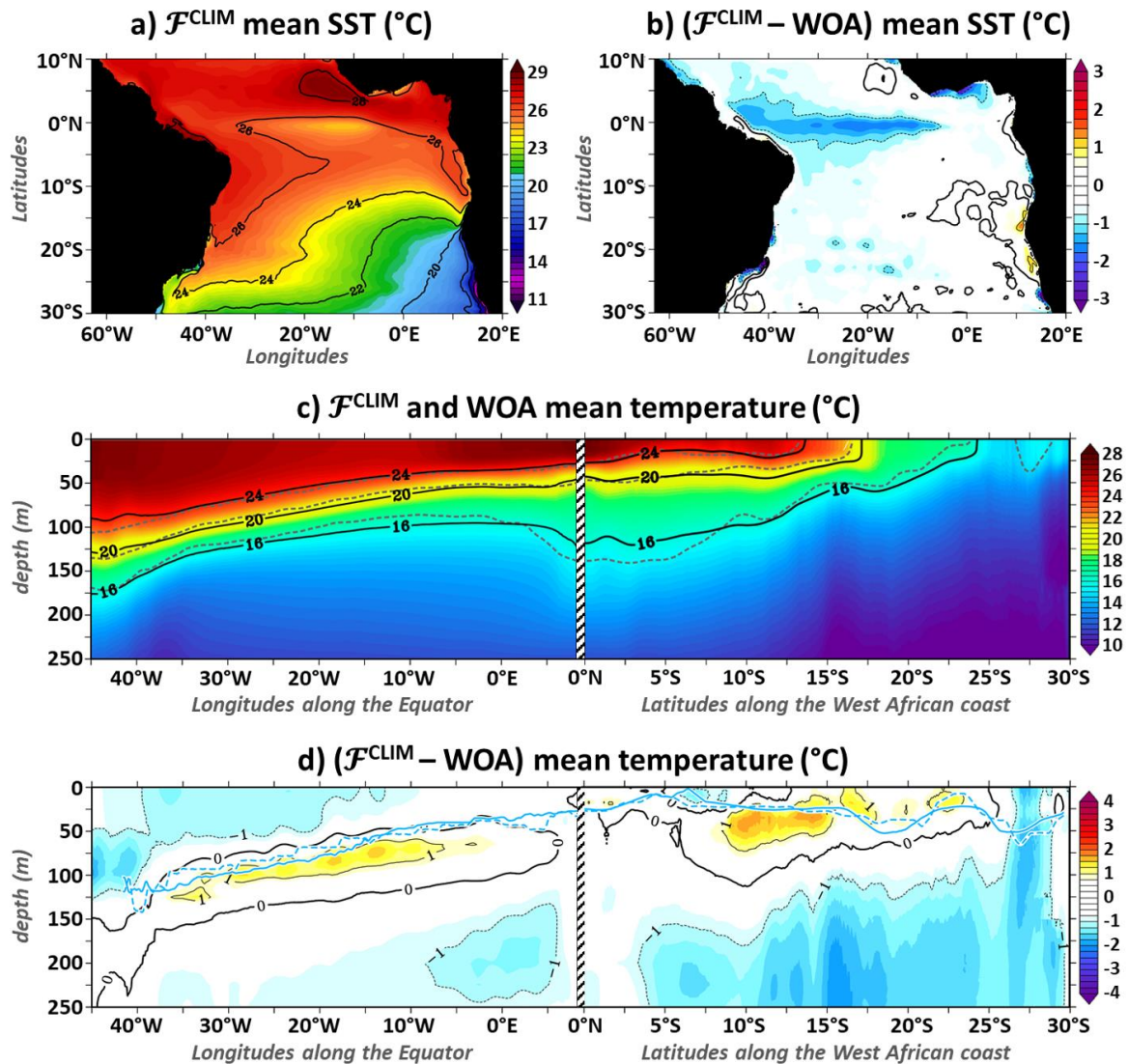


Figure S1: Comparison between $\mathcal{F}^{\text{CLIM}}$ mean temperature and WOA climatology: a) Map of $\mathcal{F}^{\text{CLIM}}$ mean temperature. b) Map of the difference between $\mathcal{F}^{\text{CLIM}}$ and WOA mean temperature. c) Vertical section of $\mathcal{F}^{\text{CLIM}}$ mean temperature along the Equator (averaged within $[3^{\circ}\text{S}-3^{\circ}\text{N}]$) and along the southwestern African coast (averaged within the 2° coastal fringe) as a function of the depth. Position of $\mathcal{F}^{\text{CLIM}}$ (WOA) 16°C , 20°C , and 24°C isotherms are highlighted using plain black (dashed grey) lines. d) Vertical section of the difference between $\mathcal{F}^{\text{CLIM}}$ and WOA mean temperature along the Equator and along the southwestern African coast as a function of the depth. $\mathcal{F}^{\text{CLIM}}$ and WOA mean positions of the thermocline (defined as the depth of the maximum vertical gradient) are depicted with plain and dashed blue lines respectively.

Unit is $^{\circ}\text{C}$.

Validation of WRF mean state from $\mathcal{F}^{\text{CLIM}}$

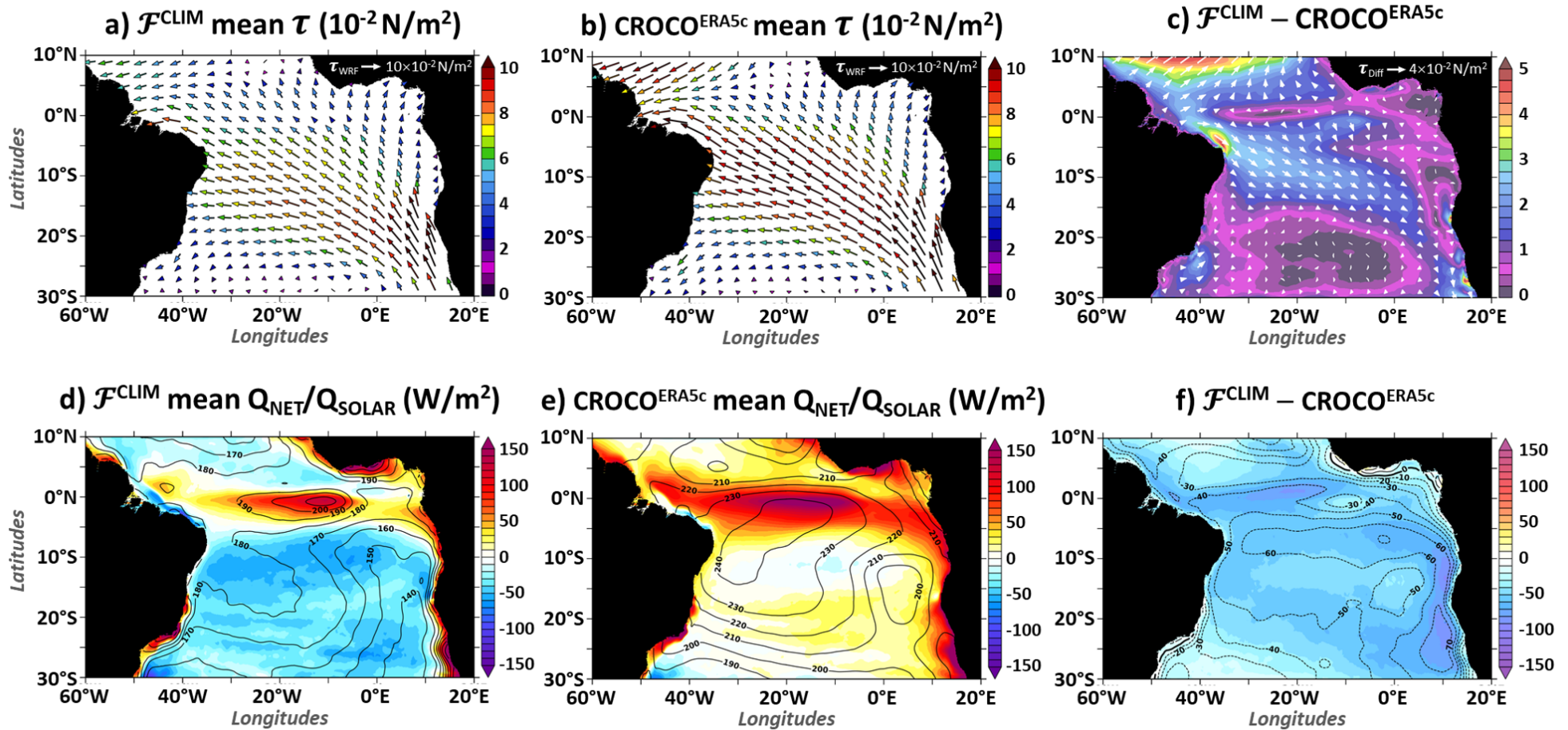


Figure S2: Comparison between $\mathcal{F}^{\text{CLIM}}$ and ERA5c (2012-2021) mean surface momentum and heat fluxes: ab) Maps of $\mathcal{F}^{\text{CLIM}}$ and ERA5c mean surface wind stress, where the color of the arrows represents the magnitude in 10^{-2} N/m^2 . c) Map of the difference between $\mathcal{F}^{\text{CLIM}}$ and ERA5c mean wind stress. de) Maps of $\mathcal{F}^{\text{CLIM}}$ and ERA5c net (colors) and solar (contours) heat fluxes in W/m^2 . f) Map of the difference between $\mathcal{F}^{\text{CLIM}}$ and ERA5c net and solar heat fluxes.

CROCO mean state in $\mathcal{F}^{\text{CLIM}}$ and $\mathcal{C}^{\text{CLIM}}$

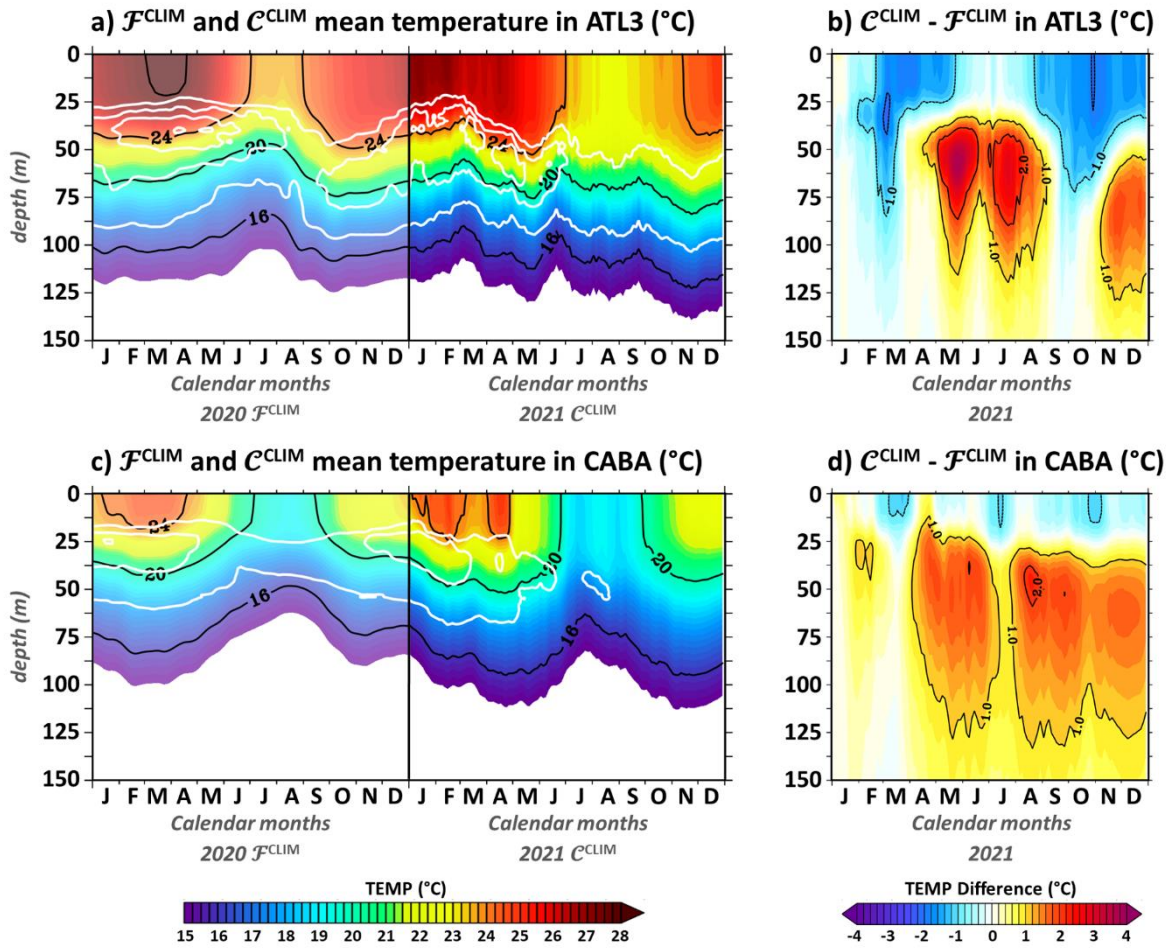


Figure S3: Comparison between $\mathcal{F}^{\text{CLIM}}$ and $\mathcal{C}^{\text{CLIM}}$ climatological ocean mean states. a) $\mathcal{F}^{\text{CLIM}}$ and $\mathcal{C}^{\text{CLIM}}$ monthly climatological temperature averaged in the ATL3 box ($[20^{\circ}\text{W}-0^{\circ}\text{E}; 3^{\circ}\text{S}-3^{\circ}\text{N}]$) as a function of the calendar months (x-axis) and the depth (y-axis). The 16°C , 20°C , and 24°C isotherms are highlighted with black lines. White lines denote the 0.1 , 0.15 , 0.2 , and 0.25 $^{\circ}\text{C}/\text{m}$ vertical temperature gradient isocontours. b) Difference between $\mathcal{F}^{\text{CLIM}}$ and $\mathcal{C}^{\text{CLIM}}$ ATL3 monthly climatological temperature. c-d) Same as panels a-b but for the CABA box ($[10^{\circ}\text{S}-20^{\circ}\text{S}, 2^{\circ}$ -wide coastal fringe]). Unit is $^{\circ}\text{C}$.

Validation of CROCO^{INTER} interannual variability

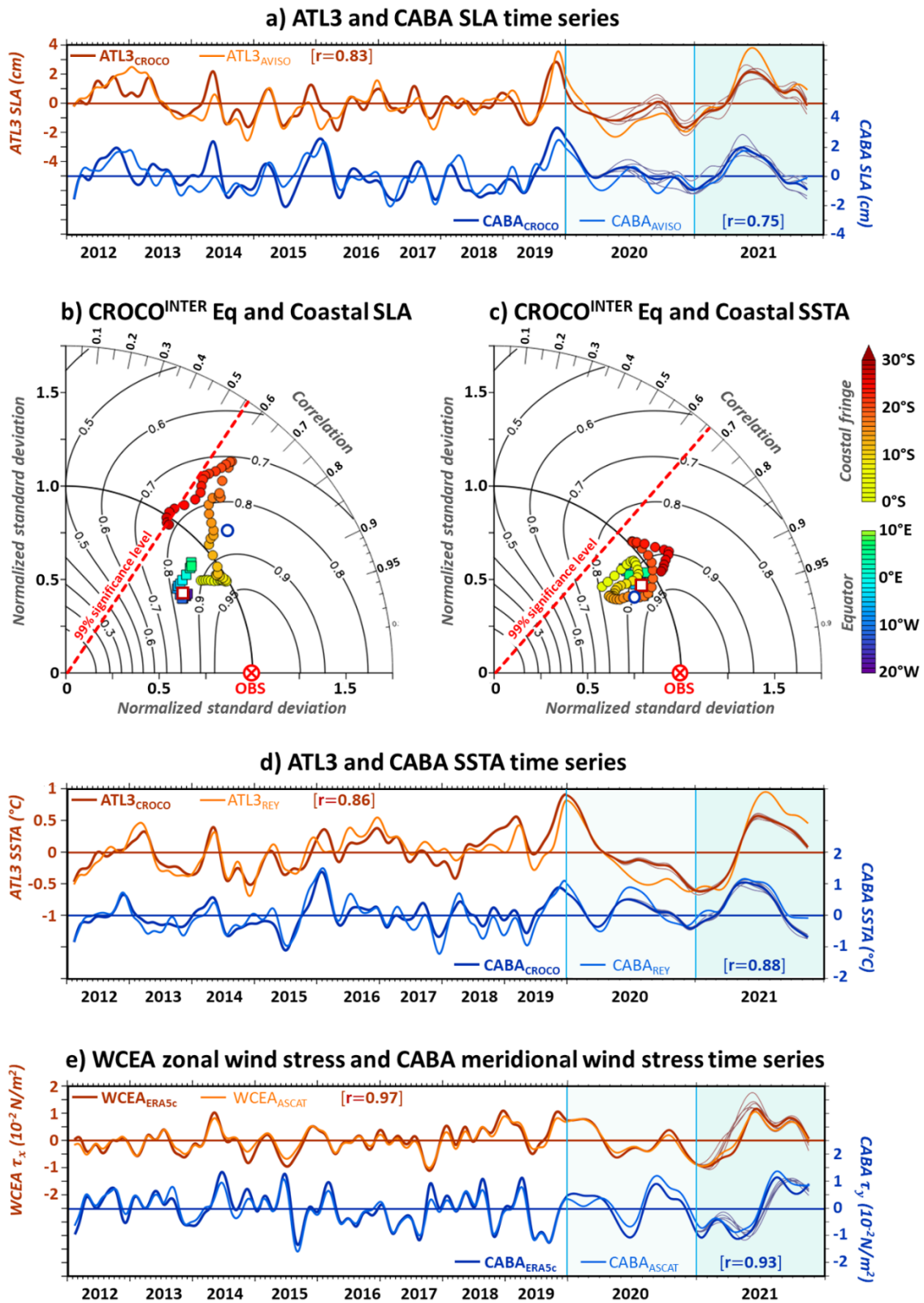


Figure S4: Comparison between CROCO^{INTER} / $\mathcal{F}^{\text{INTER}}$ and observed interannual variability over the period 2012-2021: a) detrended interannual SLA (in m) averaged in ATL3 (maroon lines, left scale) and CABA (blue lines, right scale) boxes for

CROCO^{INTER} outputs (thick dark lines) and AVISO data (thin bright lines). For the period 2020-2021, the thick dark line is the $\mathcal{F}^{\text{INTER}}$ ensemble mean and the thin grey lines are the 5 $\mathcal{F}^{\text{INTER}}$ ensemble experiments. Anomalies are computed relative to the $\mathcal{F}^{\text{CLIM}}$ ensemble mean. Unit is cm. b) Normalized Taylor diagram (Taylor 2001) illustrating CROCO^{INTER} skills in representing the altimetric interannual SLA variability from AVISO along the Equator (averaged within [3°S-3°N], solid-squares) and along the southwestern coast of Africa (averaged within the 2°-width coastal fringe, solid-circles). Colors indicate the longitude along the Equator and the latitude along the coast. Maroon open square and blue open circle are for ATL3 and CABA indexes respectively. Isolines provide a measure of the skill as defined by equation (4) from Taylor (2001). Dashed radius line denotes the limit of the 99% significance level for the correlation (Sciremammano 1979). c-d) Same as b-a) but for the quantification of the realism of CROCO^{INTER} detrended interannual SST anomalies compared to the remote-sensed OISST data. e) Interannual wind stress anomalies (in 10^{-2} N/m²) in Western Central Equatorial Atlantic (WCEA [40°W-20°W; 3°S-3°N], maroon lines, left scale) and CABA (blue lines, right scale) boxes for CROCO^{ERA5c} (thick dark lines) and ASCAT data (thin bright lines). For the period 2020-2021, the thin grey lines are the WRF wind-stress anomalies from the 5 $\mathcal{F}^{\text{INTER}}$ ensemble experiments anomalies relative to the $\mathcal{F}^{\text{CLIM}}$ ensemble mean.

The 2021 Atlantic and Benguela Niños

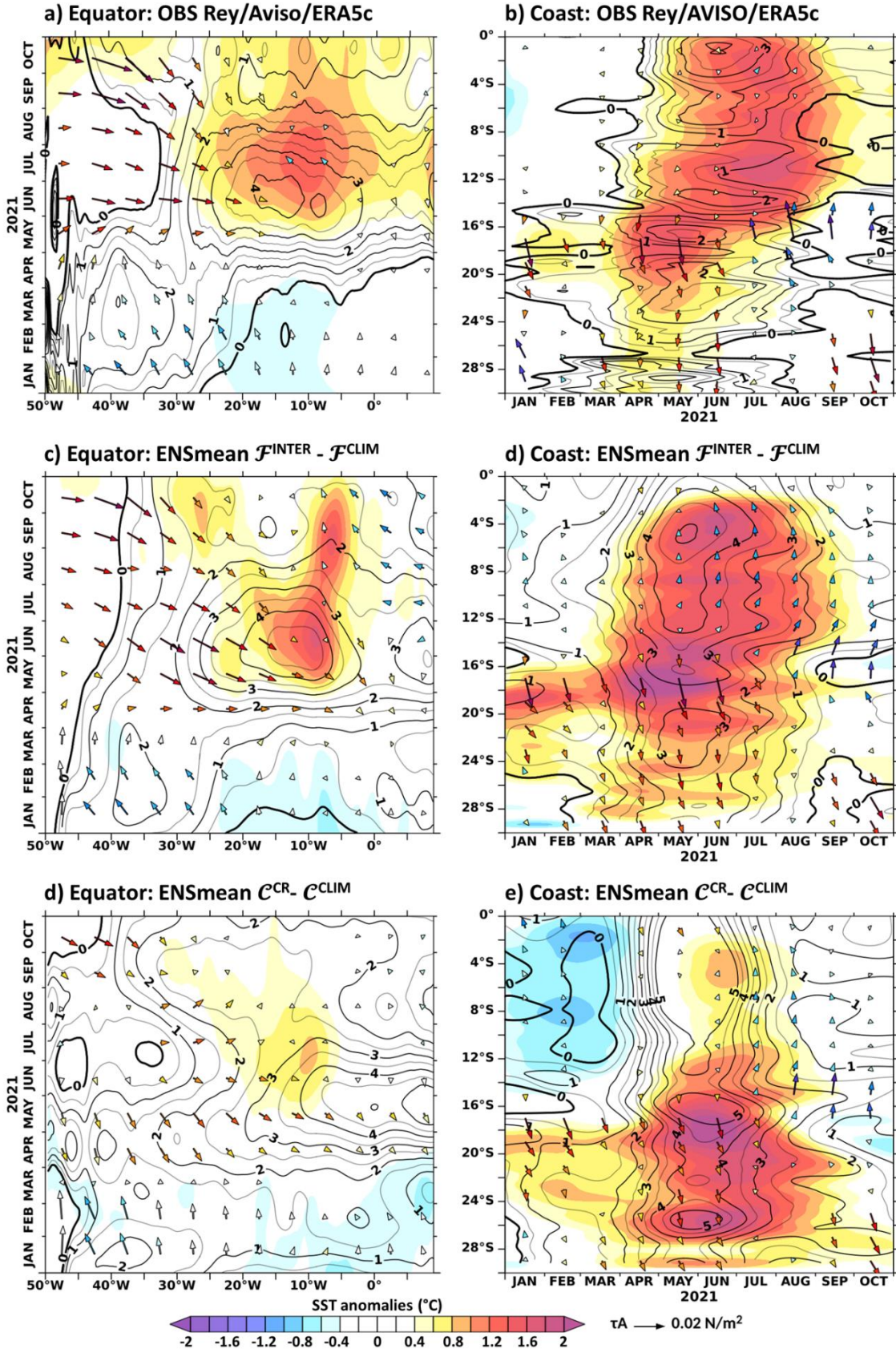


Figure S5: The 2021 Atlantic and Benguela Niño events as observed (top panels) and simulated by the forced/coupled model ensemble simulations (middle and bottom panels). a) Hovmöller plot of observed OISST data (shading, °C), AVISO SLA (contours, cm), and CROCO^{ERA5c} surface wind stress (arrows, with colors representing the zonal amplitude, N/m²) interannual anomalies averaged within the 3°S-3°N equatorial band. b) Same as panels a-b but for the ensemble mean of the forced $\mathcal{F}^{\text{INTER}}$ along the African coast, with arrow colors indicating the meridional wind-stress amplitude. cd) Same as panels a-b but for the ensemble mean of the forced $\mathcal{F}^{\text{INTER}}$ simulations, with interannual anomalies computed relative to the forced climatological simulation $\mathcal{F}^{\text{CLIM}}$. Note that, these figures are presented as **Fig.2ab** in the manuscript. ef) Same as panels ab but for the \mathcal{C}^{CR} ensemble mean, with interannual anomalies computed relative to the $\mathcal{C}^{\text{CLIM}}$ ensemble mean (same as in **Fig.5ab** of the manuscript).

Basin-scale atmospheric conditions

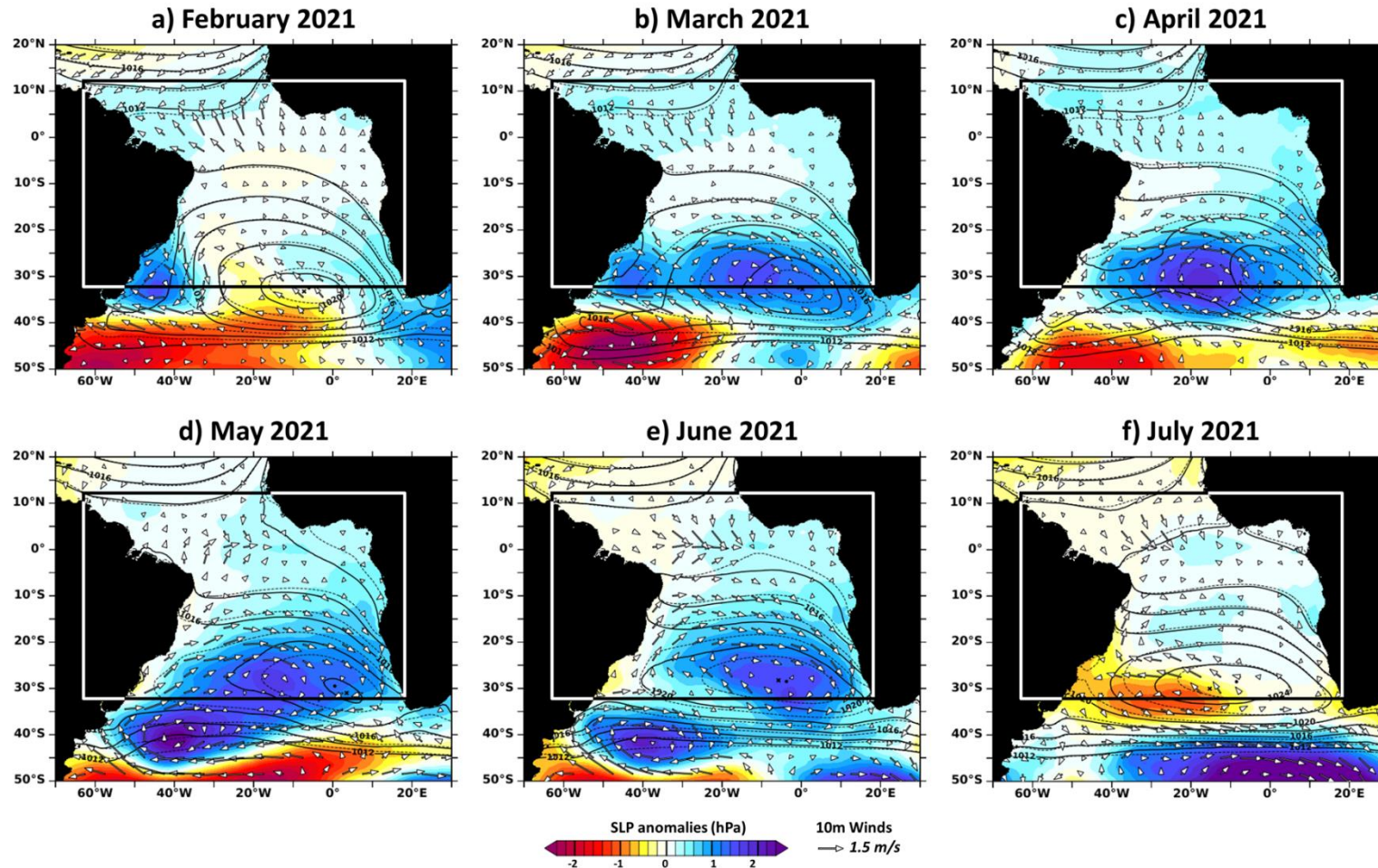


Figure S6: Basin-scale atmospheric conditions in the tropical Atlantic from February to July 2021. Sea Level Pressure (SLP) (colors, hPa) and 10-m winds (arrows, m/s) interannual anomalies. SLP is shown in solid contours, with the maximum SLP of the South Atlantic Anticyclone (SAA, 1020.2 hPa) marked with a cross, as compared to the normal conditions (dashed contours, with a dot indicating the maximum SLP of the SAA (1021.4 hPa)). The rectangle delineates our WRF atmospheric model domain.